Glomerular Elasticity and Gene Expression Patterns Define Two Phases of Alport Nephropathy

Joonho Yoon*[1], Zhenan Liu*[1], Mathew Alaba[5], Leslie A. Bruggeman[6], Paul A. Janmey[7], Carlos A. Arana[2], Oluwatoyosi Ayenuyo[8], Isabela Medeiros[8], Sean Eddy[5], Matthias Kretzler[5], Joel M. Henderson[8], Viji Nair[5], Abhijit S. Naik[$#5], Audrey N. Chang[$1,4], R. Tyler Miller[$#1,3,4]

[1]Department of Internal Medicine, University of Texas Southwestern Medical Center, Dallas Texas, USA

[2]Department of Immunology, The University of Texas Southwestern Medical Center, Dallas, Texas, 75390, USA

[3]Medicine Service, VA North Texas Health Care System, Dallas, TX, USA.

[4]Pak Center for Mineral Metabolism and Clinical Research, UTSW Medical Center, Dallas Texas, USA

[5]Department of Internal Medicine, University of Michigan, Ann Arbor, Michigan, USA.

[6]Department of Inflammation & Immunity, Lerner Research Institute, Cleveland Clinic, Cleveland, Ohio, USA

[7]Department of Physiology and Institute for Medicine and Engineering, University of Pennsylvania, Philadelphia, PA, 19104, USA.

[8]Department of Pathology and Laboratory Medicine, Boston University Chobanian & Avedisian School of Medicine and Boston Medical Center, Boston, MA, USA

[#]Corresponding authors- R. Tyler Miller, UT. Southwestern Nephrology, 8856, 5323 Harry Hines Blvd, Dallas TX 75390, 214-648-7214, tyler.miller@utsouthwestern.edu. Abhijit S. Naik, Nephrology, University of Michigan, Department of Internal Medicine, Division of Nephrology, 1500 E Medical Center Dr Fl 1, Ann Arbor, MI 48109 abhinaik@med.umich.edu

The authors have declared that no conflict of interest exists.

*Co-first authors. [$]Co-senior authors. These authors contributed equally to this work.

Abstract.

Objectives. To understand the early stages if Alport nephropathy, we characterize the structural, functional, and biophysical properties of glomerular capillaries and podocytes in *Col4α3*$^{-/-}$ mice, analyze kidney cortex transcriptional profiles at three time points, and investigate the effects of the ER stress mitigation by TUDCA on these parameters. We use human FSGS associated genes to identify molecular pathways rescued by TUDCA.

Findings. We define a disease progression timeline in *Col4α3*$^{-/-}$ mice. Podocyte injury is evident by 3 months, with glomeruli reaching maximum deformability at 4 months, associated with 40% podocytes loss, followed by progressive capillary stiffening, increasing proteinuria, reduced renal function, inflammatory infiltrates, and fibrosis from months 4 to 7. RNA sequencing at 2, 4, and 7 months reveals increased cytokine and chemokine signaling, matrix and cell injury, and activation of the TNF pathway genes by 7 months, similar to NEPTUNE FSGS cohorts. These features are suppressed by TUDCA.

Conclusions. We define two phases of *Col4α3*$^{-/-}$ nephropathy. The first is characterized by podocytopathy, increased glomerular capillary deformability and accelerated podocyte loss, and the second by increased capillary wall stiffening and renal inflammatory and profibrotic pathway activation. Disease suppression by TUDCA treatment identifies potential therapeutic targets for treating Alport and related nephropathies.

Introduction.

Many glomerular diseases including Alport nephropathy caused by mutations in *COL4A3,4, or 5,* focal sclerosing glomerulonephritis (FSGS), or Minimal Change Disease (MCD) begin with podocyte injury that is followed by varying degrees of proteinuria, hematuria, and tubulo-interstitial damage. The first evidence of podocyte injury is disruption of foot process architecture, foot process effacement, with their flattening, spreading, and loss of slit diaphragms. Further injury leads to detachment, loss of podocytes in the urine, and at some point, irreversible glomerular damage associated with tubulo-interstitial fibrosis and progression to End Stage Renal Disease (ESRD). *COL4A3,4,5* mutations, are important beyond Alport syndrome because the heterozygous state is increasingly associated with more common glomerular diseases including FSGS and IgA nephropathy and chronic kidney disease(1-4). The mechanisms that cause early podocyte injury and changes in their gene expression are not fully defined, although processes responsible for progression, focusing on tubulo-interstitial fibrosis, are increasingly understood.

Podocytes accommodate traction and shear forces and contribute to a specific biophysical environment for glomerular capillaries, all of which depend on the podocytes' unique cytoskeletal structure. Podocyte structure and function are maintained by factors including attachment to the Glomerular Basement Membrane (GBM), lateral attachment of foot processes to foot processes of neighboring podocytes, $Ca+^{2}$ fluxes, various signaling pathways, and mechanical environment (elasticity of the GBM, shear forces, and stretch)(5-12) In rats, 5/6th renal reduction causes glomerular capillary dilation to prevent increased shear stress(13). In acute and chronic glomerular injury models including Alport nephropathy, protamine, HIV nephropathy, ischemia and ischemia-reperfusion injury, the deformability of glomerular capillaries is increased as a result of podocyte injury(10, 11, 14-16). Recent intravital imaging studies show distension of glomerular capillaries and aneurisms in glomeruli from *Col4αa5*$^{-/-}$ mice at an early stage of disease, indicating increased deformability and reduced structural integrity of these capillaries at a time of accelerated podocyte loss(17-19). Loss of podocytes reflects abnormal podocyte structure with reduced adhesion that may occur due to primary podocyte injury or abnormal matrix, and these two factors may be interrelated(7, 8, 10, 11). Foot process effacement may represent a compensatory mechanism to maintain podocyte attachment to the glomerulus(20).

We used the C57BL/6J *Col4α3*$^{-/-}$ mouse model of Alport syndrome, a disease of glomerular origin, to study early steps in podocyte injury. This model retains many essential characteristics of the human disease, including accelerated podocyte loss, and has an 8-month time course allowing better time resolution of disease development and progression than other mouse strains(21-23). The abnormal GBM could injure podocytes through abnormal physical properties or abnormal signaling due to chemical differences in the normal compared to the Alport GBM(8, 24). Podocytes that produce COL4α3, 4, and 5 could be injured by accumulation of the mutant or misfolded collagen molecules with activation of the unfolded protein response (UPR, ER stress) and additional cell-specific remodeling pathways(25-27). Finally, abnormal glomerular capillary mechanics caused by disordered cytoskeletal structure could contribute to progressive podocyte injury though increased susceptibility to mechanical injury.

To distinguish among these injury mechanisms, we treated one group of *Col4α3*$^{-/-}$ mice with TauroUrsoDeoxyCholic Acid (3α,7β-Dihydroxy-5β-cholanoyltaurine, TUDCA, *Col4α3*$^{-/-}$-T), a compound that functions as a chemical chaperone and that protects cells from UPR/ER stress-mediated injury or death(28-31). We analyzed renal function, glomerular capillary elasticity, structure, and bulk renal RNA expression over the eight months of disease. We find that Alport nephropathy progresses in two phases. The first phase is characterized by podocyte injury with increasing capillary deformability and podocyte loss, while the second phase is marked by increasing proteinuria, decreasing renal excretory function, decreasing glomerular elasticity, tubulo-interstitial fibrosis, and significant increases in the expression of genes related to fibrosis and inflammation. TUDCA treatment mitigated podocyte injury and suppressed the *Col4α3*$^{-/-}$ phenotype. Furthermore, several Glomerular disease Associated Podocyte-enriched (GAP) genes identified from the NEPTUNE FSGS cohort were suppressed by TUDCA therapy in *Col4α3*$^{-/-}$ mice with the Alport phenotype. These findings thus support the role of TUDCA therapy in mitigating early podocyte injury. Furthermore, they provide knowledge of the biological, chemical and molecular pathways through which TUDCA therapy achieves this protective phenotype.

Results.

Increased glomerular capillary deformability precedes proteinuria and increased creatinine in *Col4α3*$^{-/-}$ mice. We studied the *Col4α3* mutant in the C57/Bl6 background to characterize the course of Alport nephropathy because of its relatively long time frame and the opportunity to time events accurately over 2 to 8 months. We measured serum creatinine (**Figure 1A**) and urine Albumin/Creatinine Ratio (ACR) (**Figure 1B**) beginning at 2 months of age. From 4 months, creatinine increased but did not reach statistical significance until 6 months and reached a maximum value of 61 µM at 8 months. Similarly, urine ACR increased from 0.82 at 3 months and 3.51 at 4 months to 122 at 8 months but did not reach statistical significance until 6 months. Over this time course, the serum creatinine and urine ACR values in the control mice did not change significantly.

Past work using models of acute and chronic kidney diseases showed that glomerular capillary elasticity reflects the state of podocyte cytoskeletal structure and that with podocyte injury, capillaries have increased deformability (10, 11, 16, 32). We measured glomerular elasticity (Young's modulus, E) in the control and *Col4α3*$^{-/-}$ mice from 2 to 8 months of age using micro-indentation (**Figure 1C**)(33). The values for E for both the control and *Col4a3*$^{-/-}$ mice were identical at 2 months (both 2.2 ± 0.2 kPa) and the values for the control mice remained essentially unchanged from 2 to 8 months. However, in the *Col4α3*$^{-/-}$ mice, the E values for glomeruli began to decrease at 3 months (1.85±0.09 kPa) and reached a minimum (1.56 ± 0.3 kPa) at 4 months of age. E then increased to values significantly greater than control by 7 months, reaching a maximum at 8 months (2.7 ± 0.1 kPa). These directionally opposite changes in elasticity early and late in disease signify distinctly different structural and functional properties of glomerular capillaries(10, 11, 34, 35). The early time point at which reduced glomerular E appears, before significant increases in serum creatinine and urine ACR, indicate that podocyte injury begins early in the course of renal disease, and is sufficiently severe to affect overall glomerular capillary mechanical properties.

To assess gene expression patterns in the *Col4α3*$^{-/-}$ kidneys compared to WT over the course of renal disease, we performed bulk RNAseq from renal cortex at 2, 4, and 7 months. We identified 1346 Differentially Expressed Genes (DEGs) in the 4-month WT- *Col4α3*$^{-/-}$ comparison. The top 50 increased and 50 decreased genes at 4-months from each comparison are shown in **Supplemental Tables 1-2**. The heatmaps shown in **Figure 1D and**

Supplemental Figure S1 display the expression of selected genes, grouped vertically by function, across a time course from 2 to 7 months. Each column represents an individual mouse. Visually, from 2 to 4 months, gene cluster expression patterns remain relatively stable, reflecting parallel changes in renal function and histology (see below). However, at 7 months, corresponding to parenchymal disease progression, many changes become more pronounced and statistically significant. Markers of proximal renal tubule injury, such as HAVCR1 (Kim1) and Lcn2 (NGAL), show increased expression at each time point compared to wild-type (WT) mice, with the most significant changes occurring at 7 months. Despite evidence of proximal tubular injury, EGF expression remained relatively stable until 7 months when it was halved. Genes involved in inflammation and fibrosis, including C3, Tnf, Tlr8, Thrombospondin, Ltbp2, Inhibin, Col1α1, Col1α2, Col3α1, and Lox (Lysyl oxidase), showed dramatic increases by 7 months at a time when kidney function was already deteriorating. Similar patterns were noted for various cytokines, interleukins, and chemokines (**Supplemental Figure S1** and **Supplemental Tables S3A** and **S3B**). Additionally, the expression of several kidney-specific transporters, such as Slc2a5 (Glut 5), Slc26a4 (Pendrin), Slc22a7 (OAT2), Aqp4, Slc16a4 (monocarboxylic acid transporter), and Slc12a3 (NCC), decreased significantly only at 7 months. These results indicate that significant renal parenchymal injury coincides with the onset of proteinuria after the 4-month time point in this model, while podocyte injury begins earlier.

By 4 months, markers of podocyte stress and injury were activated, as evidenced by a higher podocin:nephrin ratio (PNR) in *Col4α3*$^{-/-}$ mice compared to WT (2.45 vs. 1.367, $p<0.05$). This approach, given the cell-specific expression of podocin (Nphs2) and nephrin (Nphs1) in podocytes, is a robust way to assess podocyte injury and stress patterns despite dilution from other more abundant cell types in the renal cortex. An increased PNR reflects podocyte hypertrophic stress in studies of podocyte depletion and is linked to increased urinary podocyte detachment rates, proteinuria, and eventual kidney failure(36).

Pathway enrichment analysis of bulk-RNA seq data comparing WT and *Col4α3*$^{-/-}$ mice at 4 months identified through the Gene Expression Omnibus (GEO) demonstrated coordinated upregulation in the expression of genes associated with extracellular matrix (ECM) organization, cell-matrix adhesion, and motility to cover the increase in glomerular capillary surface area. Biological processes enriched include ECM organization

(GO:0030198), regulation of cell migration (GO:0030334), and cell-matrix adhesion (GO:0007160). Notably, there was enrichment of inflammatory response signaling (GO:0006954), cytokine-mediated signaling pathway (GO:0019221), and regulation of IL-8 production. The genes enriched in each signaling pathway are given in Supplementary Tables (https://drive.google.com/drive/folders/1nVBe2jZcjG1f31nIWa6CI5O0c7vqBP8e?usp=sharing). The affected cellular components include the collagen-containing ECM (GO:0062023), cell-substrate junction (GO:0030055), focal adhesion (GO:0005925), and basement membrane (GO:0005604). Enriched molecular functions include cytokine receptor activity (GO:0004896), consistent with the increased inflammatory response (GO:0006954), GTPase regulator activity (GO:0030695), actin binding (GO:0005509), and GTPase activator activity (GO:0005096). Thus, despite the relative lack of major changes observed at a low-resolution heatmap level, the gene enrichment pattern from cortical bulk-RNA sequencing in *Col4α3*$^{-/-}$ mice was consistent with podocyte injury, hypertrophic stress, and increased ECM and basement membrane synthesis. Additionally, there was evidence of an early inflammatory response associated with this podocyte hypertrophy and injury, as indicated by the transcriptomic data.

Evidence for unfolded protein pathway activation in *Col4α3*$^{-/-}$ podocytes. Podocytes, the cells that provide mechanical support for glomerular capillaries, determine the elastic properties of glomerular capillaries, and form the slit diaphragms, also produce and secrete the Col4α3,4,5 heterotrimer for the GBM(37). With loss-of-function mutations in any one of these proteins, podocytes must contend with inadequately processed collagen(38-40). Although referred to as a *Col4α3* knockout mouse, the mutation in this model is a truncation deleting the Col4α3 NC1 domain so that mRNA and protein presumably representing the 7S and collagenous domains are expressed (21-23). Cells compensate for excess or misfolded protein by upregulating pathways that can improve folding and/or protein degradation including Bip (HSPA5), Xbp1s (Xbp1) and CHOP (DDIT3). We imaged WT and *Col4α3*$^{-/-}$ mouse cortex with confocal microscopy and found increased Bip expression in glomerular podocytes (**Figure 2A**). The levels of Bip and Xbp1s, protein and mRNA are increased in conditionally immortalized *Col4α3*$^{-/-}$ podocytes compared to their WT counterparts (**Figure 2B**). WT cultured podocytes increase expression of Bip, Xbp1s, and CHOP in response to Tunicamycin, an agent that induces UPR, and the expression is reduced in a dose-dependent manner by treatment with TUDCA(28, 29, 31) (**Figure 2D**). Three genes related to UPR

activation were differentially expressed in the *Col4α3*$^{-/-}$ - *Col4α3*$^{-/-}$-T comparison, Xbp1 (increased 1.85 X), Dnajb9 (increased 1.50 X), and Eef1akmt3 (decreased to 0.38 X). For these reasons and expanded ER in *Col4α3*$^{-/-}$ glomerular podocytes (see Figure 7 below), we propose that an early step in podocyte injury is UPR activation with disruption of normal protein processing. If the effects of UPR activation and podocyte remodeling could be suppressed, podocyte injury could be less severe or develop more slowly.

TUDCA treatment slows progression of renal disease in *Col4α3*$^{-/-}$ mice. Although ER stress activation due to Col IV misfolding was found in cultured cell-based systems, a mouse model, and human skin fibroblasts from Alport patients, protection from renal disease by inhibition of ER stress has only been demonstrated *in vivo* recently(26, 27, 38). We tested the hypothesis that if collagen misfolding is the basis for podocyte injury in the *Col4α3*$^{-/-}$ mice, suppression of ER stress would preserve renal function and suppress disease-associated transcriptomic changes. *Col4α3*$^{-/-}$ mice were fed 0.8% TUDCA-incorporated into mouse chow from the time of weaning, 21 - 25 days old, 3 – 4 months before they developed significant proteinuria, continuously until sacrifice(41). Normal littermates served as controls. We measured the effects of TUDCA treatment on *Col4α3*$^{-/-}$ mouse serum creatinine (**Figure 3A**), urine ACR (**Figure 3B**), and the Young's elastic modulus (E) of glomeruli (**Figure 3C**) at 4 and 7 months, the nadir and peak of glomerular E (**Figure 1C**). At 4 months, serum creatinine and urine ACR values were similar among the WT, *Col4α3*$^{-/-}$, and TUDCA-treated *Col4α3*$^{-/-}$ (*Col4α3*$^{-/-}$-T) groups (**Figure 3**, left top two panels). However, at 7 months, when average serum creatinine and ACR were respectively 55±7 µm and 90±11 in the Col4α3$^{-/-}$ mice, Col4α3$^{-/-}$-T values for creatinine and ACR were respectively, 33±3.9 µm and 40±8.6. At 4 months, the value for E in the WT mice was 2.1±0.04 kPa, 1.56±0.05 kPa for the *Col4α3*$^{-/-}$ mice, and 2.0±1.0 kPa in the *Col4α3*$^{-/-}$-T mice (**Figure 3C**). At 7 months, E for WT glomeruli was 2.1±0.06 kPa, and for the *Col4α3*$^{-/-}$ glomeruli it was 2.70±0.05 kPa, while the value for the *Col4α3*$^{-/-}$-T glomeruli was 1.9±0.04 kPa, a value comparable to WT. These results demonstrate that TUDCA preserves the elastic properties of *Col4α3*$^{-/-}$ glomeruli, indicative of normalized podocyte cytoskeletal structure, reduces the severity of glomerular and parenchymal renal injury in the *Col4α3*$^{-/-}$-T mice, and implicates UPR activation in glomerular capillary injury.

TUDCA treatment preserves *Col4α3*$^{-/-}$ kidney structure. Chronic kidney disease is marked by progressive fibrosis and loss of renal function, a component of which can be attributed to proteinuria(42). Our physiologic measurements at 7 months, late-stage disease, (**Figure 3A-C**) showed preserved renal function in the *Col4α3*$^{-/-}$-T mice implying preserved glomerular and renal structure. Low magnification kidney sections from 4-month mouse kidneys stained with PAS or Picrosirius Red (PSR) show that sections from WT, *Col4α3*$^{-/-}$, and *Col4α3*$^{-/-}$-T mice are indistinguishable (**Supplemental Figure S2, also see Figure 6**), indicating that at the 4-month time point, overall renal parenchymal injury is minimal. At seven months (**Figure 3D**), the extent of injury in the Col4α3$^{-/-}$ kidneys is evident in the PAS and PSR-stained sections. Compared to the control kidneys, the PAS-stained *Col4α3*$^{-/-}$ kidneys show fibrosis, inflammatory cell infiltrates, and disrupted renal architecture. In the kidneys of *Col4α3*$^{-/-}$-T mice, these features are present, but to a significantly lesser extent. The insets show representative images of glomeruli from each group. The glomeruli from the *Col4α3*$^{-/-}$ mice are sclerotic and have excess, irregular PSR staining. Although glomeruli from the *Col4α3*$^{-/-}$-T mice are not normal, their structure is relatively preserved compared to the untreated *Col4α3*$^{-/-}$ glomeruli.

We measured the expression of genes associated with renal injury and fibrosis at 7 months using qRT-PCR of RNA samples from renal cortex in WT, *Col4α3*$^{-/-}$, and *Col4α3*$^{-/-}$-T mice (**Table 1**). In *Col4α3*$^{-/-}$ mice, expression of Col1α1, Col1α2, Col3α1, lysyl oxidase (LOX), lysyl oxidase like 2 (Loxyl2), TGF-β1, CxCl1, Ccl2, Ccr2, CN1 (Cyr61), a gene involved in development and wound healing and repair, TNFα, and IGF2, a gene involved in hypertrophy, all increased compared to WT. In the *Col4α3*$^{-/-}$-T mice, the mRNA expression for these genes was reduced to levels intermediate between those in WT and untreated *Col4α3*$^{-/-}$ mice. The reduction of TNF-α by half by TUDCA is notable because of the role of that pathway in other renal diseases(43). EGF mRNA, a marker for renal tubular health, decreased significantly (20% vs WT) in the *Col4α3*$^{-/-}$ mice compared to Control, but in *Col4α3*$^{-/-}$-T mice, EGF mRNA was expressed at an intermediate level (70% vs WT), significantly higher than in *Col4α3*$^{-/-}$ mice. These results demonstrate that TUDCA, initiated early in the course of disease, reduces glomerular injury and proteinuria, slows progression of nephropathy in *Col4α3*$^{-/-}$ mice in part by reducing cytokine and chemokine production and fibrosis, and that significant differences in the renal parenchyma between WT and Col4α3$^{-/-}$ mice are only evident after 4 months when they are associated with proteinuria, glomerular capillary stiffening and progressive renal injury.

TUDCA reduces podocyte loss from *Col4α3$^{-/-}$* mouse glomeruli. Glomerular capillaries become deformable at 3 months, before significant increases in creatinine or urine ACR, indicating that podocyte injury begins at or before that point. Alport patients lose podocytes in the urine at an accelerated rate, and podocytes can be detected in their urine before significant proteinuria develops(18, 19)**.** To identify an early time point for podocyte injury, we compared glomerular podocyte density in WT, *Col4α3$^{-/-}$*, and *Col4α3$^{-/-}$*-T mice at 2, 3, and 4 months using WT1 staining as a podocyte marker (**Figure 5**)(44). At 2 months, before reduction of glomerular E in the *Col4α3$^{-/-}$* mice, the podocyte density was similar among all three groups (Podocytes/10^6 μm^3 ± SD, WT 296±44, *Col4α3$^{-/-}$* 276±39, and *Col4α3$^{-/-}$*-T 262±45). At 3 months, when increased glomerular deformability was detectable in the *Col4α3$^{-/-}$* glomeruli, podocyte density remained unchanged in the three groups and comparable to the values for 2-month WT glomeruli (Podocytes/10^6 μm^3 ± SD, WT 285±35, Col4α3$^{-/-}$ 270±40, and Col4α3$^{-/-}$ +T 299±32). In the 3-month *Col4α3$^{-/-}$* mice, the SCr and ACR values were similar to those for the WT (SCr *Col4α3$^{-/-}$* 12.9±0.81 vs 11.4±1.0 μM and ACR *Col4α3$^{-/-}$* 0.82±0.13 vs 0.138±0.1 in WT). However, at 4 months, podocyte density was reduced in the *Col4α3$^{-/-}$* glomeruli, and TUDCA treatment protected glomeruli from podocyte loss (Podocytes/10^6 μm^3 ± SD, WT 276±48, *Col4α3$^{-/-}$* 162±37, and *Col4α3$^{-/-}$*-T 246±40). This reduction in podocyte loss from the glomeruli of *Col4α3$^{-/-}$*-T mice was accompanied by a lower PNR compared to Col4α3$^{-/-}$ mice(45). At 4 months, when SCr (*Col4α3$^{-/-}$* 14.8±-.67 vs Control 10.1±1.03) and urine ACR (*Col4α3$^{-/-}$* 3.51±0.51 vs WT 0.059±0.02) were minimally elevated, glomerular E in the *Col4α3$^{-/-}$* mice was at its lowest point, 1.56 kPa, and the podocyte density in the *Col4α3$^{-/-}$* glomeruli was sixty percent that of the WT mice.

Early glomerular capillary deformability corresponds to reduced podocyte adhesion. Based on our findings that approximately 40% of podocytes are lost in the *Col4α3$^{-/-}$* mice at 4 months (**Figure 4**), we thought that podocyte injury should be detectable at 3 months as decreased podocyte adhesion because that is the earliest detectable change in capillary elasticity, and *Col4α3$^{-/-}$* podocyte numbers are preserved. WT and *Col4α3$^{-/-}$* glomeruli had similar patterns of synaptopodin and nephrin staining indicating preserved structure at that level (**Supplemental Figure S3**). To test this possibility, we measured podocyte adhesion in 3-month-old mice as urinary podocyte loss *in vivo* in response to volume loading. Mice were injected with 0.5N saline (80 μl/g IP), and urine was collected over two hours(46). Urinary podocytes that detached and were lost into the urine were

quantified by two methods, immunoblot of urine for nephrin, a podocyte-specific protein normalized for creatinine (**Figure 5A, B**), and counting WT-1 positive cells in the urine sediment (**Figure 5C**). With acute volume loading, the amount of urinary nephrin increased four-fold over WT in the *Col4α3*$^{-/-}$ samples. TUDCA treatment reduced urine nephrin by approximately half. Urinary podocyte loss increased in *Col4α3*$^{-/-}$ mice compared to WT (**Figure 5C**). These observations were consistent in 3 different experiments, where although the number of total podocytes lost in the urine varied from mouse to mouse, only the *Col4α3*$^{-/-}$ mice had multiple WT-1 positive cells in their urine. These results show that reduced podocyte adhesion and loss begin early in nephropathy and suggest that early disease-associated structural alterations in podocytes including adhesion may contribute to the increased deformability of glomerular capillaries. TUDCA protects against podocyte loss at this early stage of nephropathy.

TUDCA protects glomerular capillary and podocyte structure. Light microscopic images of glomeruli from 4-month-old *Col4α3*$^{-/-}$ mice show generally preserved structure, but the glomeruli are hypertrophic compared to the WT mice and have multiple dilated capillaries (**Figure 6, top row**). Additionally, focal lesions are present, but there is little evidence of tubulo-interstitial damage. The *Col4α3*$^{-/-}$-T glomeruli show evidence of focal lesions and capillary dilation, but considerably less than the *Col4α3*$^{-/-}$ glomeruli, and have no evidence of hypertrophy. At 7 months, the patterns described above persist but in the *Col4α3*$^{-/-}$ mice are more severe with more glomerulosclerosis, focal glomerular lesions, and significant tubulo-interstitial injury and inflammation. The *Col4α3*$^{-/-}$-T kidneys show less glomerular and tubulo-interstitial injury compared to the *Col4α3*$^{-/-}$ kidneys, but injury progressed from the 4-month time point (**Supplemental Table S4**).

We used transmission electron microscopy (TEM) to compare podocyte and GBM structures in our three groups of mice at 4 and 7 months (**Figure 7**). At 4 months, the glomeruli from the *Col4α3*$^{-/-}$ mice show regions of irregular GBM structure with thin and thick regions. The podocyte foot processes are normal in some regions but also show evidence of effacement and widening in other regions. Some podocyte cell bodies appear hypertrophic, exhibiting vacuolization, and have expanded ER indicative of ER stress, and microvillus formation (**Supplemental Figure S4, Supplemental Table S5**. In the *Col4α3*$^{-/-}$-T glomeruli, these pathologic findings are present, but less severe than in the Col4α3$^{-/-}$ mice. By 7 months, the pathologic changes in the *Col4α3*$^{-/-}$ GBMs

and podocytes are more advanced with evidence of substantial glomerulosclerosis. The *Col4α3*$^{-/-}$-T glomeruli have characteristics intermediate between the WT and Col4α3$^{-/-}$ glomeruli. The pathologic findings are quantified in **Supplemental Table S5**.

Gene expression patterns in Col4α3$^{-/-}$ vs WT mice. In untreated *Col4α3*$^{-/-}$ mice compared to TUDCA-treated *Col4α3*$^{-/-}$ mice, Gene Ontology analysis revealed enrichment for molecular functions including phosphatidylinositol transfer (GO:0008526), filamin binding (GO:0031005), and inhibitors of metalloendopeptidase activity (GO:0008191). Enriched biological processes included podocyte development (GO:0072015), cell migration (GO:0030334), and podocyte differentiation (GO:0072112). Enriched cellular components gene groups included collagen-containing extracellular matrix (GO:0062023), basement membrane (GO:0005604), and microvillous formation (GO:0031528). This pattern is similar to the enrichment observed between *Col4α3*$^{-/-}$ and WT animals. The drive to increase ECM and basement membrane synthesis was evident, alongside increased expression of inhibitors of Metall endopeptidase activity to presumably prevent the degradation of existing and newly synthesized ECM. Podocyte differentiation may reflect podocyte hypertrophy. Additionally, there was increased expression of genes associated with epithelial to mesenchymal transition (GO:0010717), indicating ongoing podocyte injury. This ongoing injury was further supported by decreased expression of transcripts associated with glycerophospholipid and lipid synthesis, suggesting that cells were reducing energy-consuming biosynthetic activities to support growth. TUDCA therapy that rescued the Alport phenotype had lower enrichment for the genes described above.

Correspondence between proteinuria-associated genes in mouse and human datasets. To test whether the molecular signatures associated with glomerular disease progression are relevant to clinically meaningful outcomes in humans, we performed a cross-species comparison. We identified genes associated with proteinuria in 7-month *Col4α3*$^{-/-}$ mice and then mapped these genes to human RNA-seq data from a recently published NEPTUNE cohort which includes patients with FSGS and Minimal Change Disease (MCD)(43). The rationale for choosing the 7-month timepoint was its phenotypic match to a disease state similar to what is seen in pediatric and adult nephrology clinics. An Independent Component Analysis (ICA) using the 7-month RNA-

seq data from *Col4α3*$^{-/-}$ mice identified a set of 253 genes in a module (IC6) associated with proteinuria ($p<0.05$) – Is this the way to state it?. The proteinuria-associated genes in our *Col4a3*$^{-/-}$ model were strongly enriched in the top 10% of overexpressed genes from micro-dissected glomerular bulk-RNA seq data of FSGS patients comparing nephrotic with sub-nephrotic range proteinuria in the NEPTUNE cohort (p=1.22E-6; q=5.11E4, Odds Ratio: 2.6)(43). **Supplemental Table S7** shows RT-PCR validation of expression of selected genes from the NEPTUNE cohort (Lif, Krt19, C3, FosB, Vcan, and Egr1) in the 7 Month *Col4α3*$^{-/-}$ mouse data. Not only did these genes change in the same direction in the *Col4α3*$^{-/-}$ mouse data, but the increases were suppressed by TUDCA. The paper by Mariani et al also showed increased expression of TNF-α signaling pathway genes in patients with FSGS and MCD and poor outcomes(43). We used the upstream activators and downstream targets of TNF signaling identified in that work to assess TNF pathway activity in our Col4α4$^{-/-}$ mouse kidney RNA samples. At 7 months, mRNAs coding for the TNF pathway activators and TNF targets are significantly increased in the Col4α4$^{-/-}$ mice compared to WT (**Figure 2A, B**)(43). At 7 months, TUDCA suppressed TNF-α expression by 50% (**Table 1**). However, TNF-α, like many other genes associated with inflammation and its upstream activators and downstream targets was not significantly increased or not differentially expressed at 2 and 4 months (**Table 2A, 2B, Supplementary Tables 3A, 3B**). These results indicate that not only does the Alport nephropathy mouse model express genes associated with proteinuria in human renal biopsies of patients with glomerular disease, but that a subset of genes that have pathologenic roles in glomerular disease are shared between these two datasets, and that in the *Col4α3*$^{-/-}$ mice, the magnitude of the change correlates with the stage of the disease. Of particular interest, the expression of many of these genes is changed by TUDCA in a direction consistent with suppression of the Alport phenotype.

Discussion.

We followed the course of nephropathy in *Col4α3*$^{-/-}$ mice (C57Bl6 strain) from 2 to 8 months of age to identify mechanisms of renal injury at early time points. We assessed renal function and structure as well as glomerular capillary and podocyte structure, function, elastic properties, and gene expression. We have three principal findings. First, in *Col4α3*$^{-/-}$ mice, Alport nephropathy has two distinct phases. In the first phase, from birth through 4 months, podocyte injury and loss occur in the absence of significant proteinuria, reduced renal function, or tubulo-interstitial injury. Evidence of podocyte injury includes increased deformability of glomerular capillaries, reduced adhesion of podocytes to glomerular capillaries, early foot process effacement, and podocyte loss. This increased deformability probably sensitizes the capillaries to mechanical hemodynamic injury further accelerating podocyte loss. Podocyte stress, hypertrophy, and injury pathways are activated in response. This phase may represent reversible disease. The second phase, from 4 to 7 months following the loss of approximately 40% of podocytes, is characterized by increasing rigidity of glomerular capillaries, progressive proteinuria and tubulo-interstitial fibrosis with activation of genes associated with progressive glomerulosclerosis, and tubulo-interstitial fibrosis with decreasing expression of differentiated genes related to renal transport function. The expression of many inflammatory mediators, largely absent at 2 and 4 months, increases significantly during this time. This second phase may represent irreversible disease.

The second major finding is that TUDCA, an agent that reduces the consequences of UPR activation, significantly slowed the progression of renal disease in *Col4α3*$^{-/-}$ mice by ameliorating podocyte injury and stress, resulting in a 50% reduction in serum creatinine, 65% reduction in urine ACR, and near normalization of glomerular capillary E at 7 months. This and one other recent publication demonstrate that interfering with UPR activation suppresses the Alport renal disease phenotype and implicates the UPR pathway in the pathogenesis of the disease(26).

Third, we found that TUDCA changed the expression of 60 of the 327 podocyte enriched genes in the opposite direction from the untreated *Col4α3*$^{-/-}$ mice. Many of these TUDCA-responsive podocyte-enriched genes also had their expression patterns reversed in the *Col4α3*$^{-/-}$ model of Alport nephropathy using a different mouse strain, Svj129 X Bl6 Fi hybrid, and two distinct treatments (ACEi and anti-miR-21)(47). These results suggest

that the human podocyte injury-enriched gene set we identified is mechanistically related to podocyte injury and progression in currently available Alport model systems, and further suggest that these models accurately recapitulate disease-associated gene expression and responses to treatment among genes relevant to human disease. Furthermore, in 7-month *Col4α3*$^{-/-}$ mice, we identify a gene expression pattern characteristic of TNF-α activation that is also found in a NEPTUNE cohort of FSGS and MCD patients, further demonstrating the relevance if the *Col4α3*$^{-/-}$ model to human disease(43).

Podocyte injury, hypertrophy in response to podocyte loss, or other hypertrophic stimuli can cause increased capillary deformability that may represent a podocyte-specific remodeling program (10, 11, 16, 48-50) The first observed step in podocyte injury is rearrangement of podocyte cytoskeletal structures with effacement of foot processes, ultimately leading to loss, so a difference between the biophysical properties of effaced or injured and normal podocytes is a reasonable expectation. Increased podocyte and capillary deformability may predispose to mechanical trauma and accelerate glomerular failure. This idea is consistent with the beneficial effect of ACEi/ARB therapy(47, 50, 51). Our finding of increased capillary deformability in the *Col4α3*$^{-/-}$ mouse model is supported by studies of Gyarmati et al, who found dilated glomerular capillaries with aneurisms and thrombi in early-stage Col4α5$^{-/-}$ KO mice (C57/Bl6 background), similar to our results where capillary deformability was measured directly (17). Podocyte hypertrophy, also present in our *Col4α3*$^{-/-}$ mice, is sufficient to increase the deformability of podocytes and glomerular capillaries. Cortes et al perfused glomeruli from control and remnant rat kidneys with hypertrophic glomeruli at progressively increasing pressures over the physiologic range and calculated values for compliance. Conversion of compliance to E yields a value 2.3 kPa in control glomeruli that is similar to ours, 2.2 kPa. The remnant kidney glomerular E decreased by 40% to approximately 1.4 kPa, a value similar to 1.56 kPa seen in our 4-month-old *Col4α3*$^{-/-}$ mice (11, 48). These results indicate that the GBM in early Alport nephropathy is not rigid, does not determine the distensibility of glomerular capillaries, and that podocyte structure is more likely to have the dominant effect on capillary deformability. In this setting, even normal blood pressure is likely to injure podocytes and hypertension would be even more damaging(45). Capillary deformability could be a therapeutic target.

The relationship between podocyte and GBM structure, and the mechanical integrity of glomerular capillaries is not fully defined. In short-term studies where the structure of the GBM is unlikely to change, reinforcement of the actin cytoskeleton with agents such as Jasplakinolide or high Mg that increases Integrin affinity and F-actin, or WNK1 kinase activation reduces capillary deformability (increases rigidity)(10, 11, 32, 35). Conversely, chemical disruption of the podocyte cytoskeleton with actin depolymerizing agents, protamine, WNK1 kinase inhibition, or ischemia-reperfusion injury increase deformability. These results demonstrate an essential role for podocytes in determining capillary wall mechanical properties(10, 11, 35). ER stress like other forms of cell injury is likely to disrupt cytoskeletal structure. Elastic environment and the mechanical behavior of neighboring podocytes can affect their mechanical properties independently of the nature of the matrix(6, 10). In genetic experiments, the structure of the integrin-linked cytoskeleton affects matrix composition by a mechanism involving recruitment of α-actinin-4 and PDLIM-5 to adhesomes by EPB41L5(24). Reduced recruitment of these proteins results in decreased adhesion strength and synthesis of matrix components, and increased recruitment has opposite effects(8). Inflammatory injury of other glomerular cells may also contribute to podocyte injury(17). All of these factors probably contribute to aggregate tissue elastic properties and represent an integrated cellular response to injury that predisposes to mechanical injury. This form of injury may be amenable to interventions beyond ACEi/ARB therapy.

Until recently, showing a benefit of UPR suppression on the course of Alport nephropathy in vivo has been difficult (Pers. Comm Jeff Miner)(26, 27, 38). Several factors may contribute to this situation. First, podocyte injury probably begins with expression of the disrupted *Col4α3,4,5* heterotrimer before or near birth, long before clinical evidence of disease, and accelerates with birth and post-natal renal perfusion(37, 52). Our intervention began at the time of weaning, 4 weeks after birth and resulted in a 50% reduction in serum creatinine, 65% reduction in urine ACR, and preservation for glomerular capillary E. If interventions start with the onset of “clinical” evidence of renal disease, 4 – 6 months in the Bl6 model, sufficient injury is present that renal function may not be stabilized, or its rate of loss not slowed. In models that progress more rapidly such as the SvJ strain or with severe mutations such as the *Col4α5* G5X mutation, proteinuria and renal failure occur earlier, compressing the course of disease. In that case, interventions could occur relatively late in the disease course with more severe preexisting pathology when treatment starts, and the ability to see treatment responses may

be limited(22, 53). The mouse model studied by Yu et al was in the Bl6 strain and they started TUDCA at 4 months. However, their mutation, Col4α3 G799R appears to be a milder phenotype than ours with deletion of the Col4α3 NC1 domain(26). Nevertheless, Rubel et al initiated ACEI therapy at 4 weeks and anti miR-21 therapy at 6 weeks, a later stage of disease than in our studies, and found comparable benefit(47). The magnitude and nature of the effect of anti miR-21 and synergistic effects of ACEI treatment may be responsible for the success of their approach, and the effect was more pronounced in the more slowly progressing F1 hybrid Svj126 X Bl6 *Col4α3*$^{-/-}$ mice(47).

Gale et all recently reported a randomized controlled trial of anti miR21 in adult Alport patients that was stopped for lack of effect(54). The patients began treatment with a mean eGFR value of approximately 55 ml/min/1.73 m^2/yr, an eGFR slope of ˜8 ml/min/1.73 m^2/yr, and mean UACR value of 2681. Proteinuria did not change with treatment. These patients had disease that is probably equivalent to our 6-month-old mice with significant loss of GFR, podocyte loss, glomerular hypertrophy, and established tubulo-interstitial fibrosis and inflammation. Disease advanced to that extent is less likely to respond to treatment than if it had been started earlier.

TUDCA suppresses the effects of UPR activation, and in these studies preserves glomerular and renal function. Although UPR activation in podocytes appears to be an early step in Alport nephropathy, it probably initiates distinct, later processes involved in progression and different processes in other cell types. Thus, disease progression and each cell type could have their own disease trajectory that could be altered with other external noxious stimuli. This lends itself to targeted therapies to processes such as endothelial injury and fibrosis driven by IL-11 which we see increased at 7 months(17, 55). These beneficial effects of TUDCA may derive from improved podocyte function as suggested by our transcriptomic analysis, but TUDCA may also have additional effects including suppression of inflammation. (26, 30, 56, 57). It is however possible that the reduction in inflammation is the result of decreased podocyte injury which begets lesser activation of the innate immune response. UPR activation with mitochondrial injury initiates the UPR which in turn can activate the integrated stress response (ISR) that includes the innate immune pathway(58, 59). In our data, many RNAs associated with these processes were suppressed by TUDCA but whether that is a primary effect or secondary to improved podocyte function, possibly as a result or reduced proteinuria, is unclear(42). The connections between initial

injury and progression pathways remain to be defined, and future single cell studies should begin to resolve these questions.

In *Col4α3*$^{-/-}$ mice, we found that Alport nephropathy progresses through an early phase defined by podocyte injury and loss followed by a later phase characterized by overt proteinuria, inflammation, and fibrosis. TUDCA, a bile acid derivative that suppressed the effects of UPR activation suppressed the Alport phenotype and reversed or minimized gene expression changes characteristic of the late phase of disease. This pattern of gene expression may represent an early, but general response to podocyte injury so it may have relevance to other diseases with podocyte injury, particularly FSGS and IgA Nephropathy with *Col4α3,4,5* mutations and heterozygous states(3). To the extent that UPR activation is a component of other podocyte and glomerular diseases, these gene sets may be relevant to developing treatments. Podocyte injury and downstream renal injury could be mitigated by TUDCA or by targeting its downstream signaling pathways if initiated early before disease is established and irreversible.

Methods.

Reagents. All fluorescent antibodies were purchased from Invitrogen. *Antibodies for immunofluorescence* **-** Col4α3: (Rat) Clone H31 97076), Chondrex, Inc.; Col4α3: (Rabbit) MBS2026491, BioSource; Bip: ab21685, Abcam; WT-1: sc-7385, Santa Cruz; Synaptopodin: sc-21537, Santa Cruz; Nephrin: AF3169, R&D Systems. *Antibodies for immunoblotting* - Bip: ab21685, Abcam; Xbp1s: sc-7160, Cell signaling, and 24868-1-AP, Proteintech; Chop: (D46F1), #5554, Cell Signaling; GAPDH: XP, #5174S, Cell signaling; β-actin – #AM4302 Invitrogen.

Mouse breeding and treatment. Col4α3$^{-/-}$ mice in the C57Bl/6J background were obtained from Jeff Miner(22). Genotyping was performed by Transnetyx. For studies, homozygous males were bred with heterozygous females to obtain Col4α3$^{-/-}$ and Col4α3$^{+/+}$ mice. KO mice were fed 0.8% TauroUrsoDeoxyCholic Acid, 3α,7β-Dihydroxy-5β-cholanoyltaurine (TUDCA) incorporated into mouse chow from the time of weaning (25-28 days old) until sacrifice (28, 29, 31, 41). TUDCA (98% purity) was from Chemimpex and was incorporated into standard mouse chow by Teklad. Normal littermates served as controls.

We measured the serum creatinine either by submandibular puncture or exsanguination at the time of sacrifice. After clotting at room temperature for 1hr and centrifugation at 2000 x g for 10min, the supernatants were transferred to new clean tubes and stored at -80 °C for further analysis. Mouse urine samples were collected from spot urine in clean empty cages and centrifuged at 400 x g for 10min. The supernatant was transferred to new, clean tubes and stored at -80 °C. Urine albumin concentrations were measured using a Mouse Albumin ELISA Kit (Immunology Consultants Laboratory, Inc). Serum and urine creatinine levels were measured by UTSW O'Brien Kidney Research Center Physiology Core using capillary electrophoresis. Urine albumin-to-creatinine ratios were calculated to assess the severity of albuminuria.

Podocyte adhesion was measured in vivo by injecting 0.5N saline (80 µl/g IP) and collecting urine over two hours(46). An aliquot of urine was normalized for creatinine and immunoblotted for nephrin. Another aliquot was centrifuged, the sediment attached to a slide and stained for DAPI and WT-1.

Isolation of mouse glomeruli. To isolate glomeruli, kidneys were removed from mice, placed in iced buffer, decapsulated, and dissected on ice to isolate the cortices from the medullae. The cortices were minced with a

razor blade and pushed through a screen (180 μm, W.S. Tyler Co, Cleveland, OH) with a flexible metal spatula. The minced tissue was suspended in PBS with 5.5 mM glucose and 0.3 mM pyruvate (GIBCO), filtered through a 90 μm nylon mesh (Falcon) to remove vessels and large pieces of tissue. The filtrate was collected in a 45 μm mesh nylon filter (Falcon) and contained intact glomeruli with minimal contamination (< 2%) by tubular cells(10, 11, 60). Glomeruli were maintained in DMEM with 0.1% FBS at room temperature before drug treatment, elasticity measurements or confocal imaging.

Podocyte cell line development and culture. Podocyte cell lines were derived from WT and Col4□3$^{-/-}$ primary podocyte outgrowths from glomeruli isolated from adult mice (12-16 weeks of age). Glomeruli were maintained in DMEM with 0.1% FBS at room temperature and seeded onto collagen I-coated dishes for 4-6 days to allow primary glomerular cell outgrowth. Primary podocytes were then trypsinized, filtered with 20 μm cell strainer, and re-plated for experiments or immortalization. Primary podocytes were conditionally immortalized by infection with a lentivirus expressing the temperature sensitive SV40 T antigen tsA58. Lentivirus was produced from pLenti-SV40-T-tsA58 (abm cat# LV629) as previously described (61) using the VSV envelope from pMD2.G (Addgene cat#12259, gift from Didier Trono) and the packaging plasmid pCMV delta R8.2 (Addgene cat # 12263, gift from Didier Trono). Primary glomerular outgrowths were infected for 48 hours followed by selection with puromycin (2ug/ml). Conditionally immortalized mouse podocytes were cultured in RPMI 1640 with 10% FBS. Cells cultures were expanded at 33°C and for experiments, differentiated at 37°C for 7-10 days as previously described (62).

Animal Studies. Animal research was performed in accordance with the UT Southwestern Medical Center Animal IACUC guidelines. The research study protocol (number 2014-0078) was approved by the UT Southwestern Medical Center Animal IACUC (NIH OLAW Assurance Number A3472-01). UT Southwestern Medical Center is fully accredited by the American Association for the Assessment and Accreditation of Laboratory Care, International (AAALAC). Animals are housed and maintained in accordance with the applicable portions of the Animal Welfare Act and the Guide for the Care and Use of Laboratory Animals. Veterinary care is under the direction of a full-time veterinarian boarded by the American College of Laboratory Animal Medicine. Mice were sacrificed for experiments by first anesthetizing with Avertin and then euthanizing by exsanguination.

Kidney total RNA sample preparation for RNAseq. Kidneys from each group of mice were removed and 20 mg of cortex was processed for RNA purification. All samples were stored with RNA later in -80 °C and thawed for RNA purification. Total RNA was purified using Direct-Zol™ RNA Miniprep Plus (Zymo research) and the concentration was measured with DS-11 FX+ (Denovix). Final RNA samples were submitted for sequencing to Next Generation Sequencing Core of UTSW. Sequence analysis and results were performed by the University of Michigan Nephrotic Syndrome Study Network (NEPTUNE).

Quantitative RT-PCR. Total RNAs were purified from each group of mouse cortex part using Direct-Zol™ RNA Miniprep Plus (Zymo research) and used for reverse transcription by SuperScript III First-Strand Synthesis System (Invitrogen). Quantitative PCR was carried out with specific primers using SYBR™ Green PCR Master Mix (Applied Biosystems) and StepOnePlus™ Real-Time PCR System (Applied Biosystems). For quantitative analysis, the samples were normalized to GAPDH (Glyceraldehyde 3-phosphate dehydrogenase) gene expression using the ΔΔCT value method. Primer sequences for specific genes are below.

C3 forward: 5'-CGCAACGAACAGGTGGAGATCA, reverse: 5'-CTGGAAGTAGCGATTCTTGGCG-3'

Ccl2 forward: 5'-GCTACAAGAGGATCACCAGCAG-3', reverse: 5'-GTCTGGACCCATTCCTTCTTGG-3'

Ccr2 forward: 5'-GCTGTGTTTGCCTCTCTACCAG-3', reverse: 5'-CAAGTAGAGGCAGGATCAGGCT-3'

Cxcl1 forward: 5'-TCCAGAGCTTGAAGGTGTTGCC-3', reverse: 5'-AACCAAGGGAGCTTCAGGGTCA-3'

Col1α1 forward: 5'-GGAGAGAGCATGACCGATGG-3', reverse: 5'-AAGTTCCGGTGTGACTCGTG-3'

Col1α2 forward: 5'-GCTGGTGTAATGGGTCCTCC-3', reverse: 5'-ATCCGATGTTGCCAGCTTCA-3'

Col3α1 forward: 5'-AGGCTGAAGGAAACAGCAA-3', Col3α1 reverse: 5'-TAGTCTCATTGCTTGCGTG-3'

Col4a3 forward: 5'-CAAAGGCATCAGGGGAATAACT-3' (aa-88, N-terminal region, 7S domain), 5'-ATTAGTGGCAGAGCTCTCG-3' (NC-1 domain), reverse: 5'-ACCCTTAGATCCGTTGCATCC-3'

Col4a4 forward: 5'-TTTGGACAGGGTACAGCTTG, reverse: 5'-TAGTGGCACACTTGGTGGAT

Col4a5 forward: 5'-CTGGAAGAATGGGTCCAGAT, reverse: 5'-GTTCCTTTGAAACCTGGGAA

Cyr61 forward: 5'-GTGAAGTGCGTCCTTGTGGACA-3', reverse: 5'-CTTGACACTGGAGCATCCTGCA-3'

EGF forward: 5'-ATCTGACTTCATGGAGACA-3', reverse: 5'-AACTGGCTCTGTCTGCCGT-3'

Egr1 forward: 5'-AGCGAACAACCCTATGAGCACC-3', reverse: 5'-ATGGGAGGCAACCGAGTCGTTT-3'

FosB forward: 5'-ACCTGTCTTCGGTGGACTCCTT-3', reverse: 5'-TGGCTGGTTGTGATTGCGGTGA-3'

GAPDH forward: 5'-CCATGGAGAAGGCTGGGG-3', reverse: 5'-CAAAGTTGTCATGGATGACC-3'

Lif forward: 5'-TCAACTGGCACAGCTCAATGGC-3', reverse: 5'-GGAAGTCTGTCATGTTAGGCGC-3'

LOX forward: 5'-CCGGTTACTTCCAGTACGGT-3', reverse: 5'-ATCCGCCCTATATGCTGAAC-3'

LOXL2 forward: 5'-GGAAAGCCTACAAGCCAGAG-3', reverse: 5'-GCAGATACCAGGTCCCACTT-3'

TNFα forward: 5'-ACGTCGTAGCAAACCACCA-3', reverse: 5'-TTGTCCCTTGAAGAAAACCT-3'

TGFβ-1 forward: 5'-CAGTGGCTGAACCAAGGAG-3', reverse: 5'-ATCCCGTTGATTCCAGGTG-3'

Vcan forward: 5'-GGACCAAGTTCCACCCTGACAT-3', reverse: 5'-CTTCACTGCAAGGTTCCTCTTCT-3'

Measurement of glomerular elasticity. The elastic moduli of glomeruli isolated from 3–6-month-old mice were measured using a microprobe indenter device(10, 11, 33). Briefly, a tensiometer probe (Kibron, Inc, Helsinki) with a 250 µm radius flat-bottom needle was mounted on a 3-D micromanipulator with 160 nm step size (Eppendorf, Inc) attached to a Leica inverted microscope. A glass slide containing a dilute sample of glomeruli was imaged by bright field illumination and the bottom of the probe was brought through the air-water interface until it was just above the surface of a single glomerulus of diameter approximately 60 µm. The probe was calibrated using the known surface tension of a pure water/air interface, and the stress applied to the probe as it was lowered onto the glomerulus was measured as a function of indentation depth. In principle, this deformation geometry is that of an infinite plane compressing a spherical object. The absolute values of elastic modulus can be calculated from appropriate models that require assumptions about the adherence of the glomerulus to the probe and the glass slide, whether the glomerular elasticity is modeled as a uniform sphere or an elastic shell, and other structural factors that confound calculation of the magnitude of elastic modulus from the force-indentation data alone. In all cases indentations were kept below 15 µm to avoid large strains that could damage the glomeruli. After the largest indentations, measurements were repeated at small strains to confirm that the deformations were recoverable.

Light microscopy of renal tissue. Formalin-fixed, paraffin-embedded kidney tissue was sectioned at 3 µm, and sections were stained with periodic acid-Schiff or picrosirius red stains. Stained tissue sections were examined, and digital images were collected under brightfield microscopy with an Olympus BX-80 microscope equipped with a Q-Imaging Retiga 2000R imaging system.

Immunofluorescence staining. Treated glomeruli were spun down at 5,000g for 5 min, resuspended and fixed in 4% paraformaldehyde for 30 minutes, and then washed 3x in PBS. Washed glomeruli were resuspended in PBS, 100 □l pipetted onto a slide, and attached to a coverslip overnight at 4˚C. The slide was rinsed in PBS to

remove unattached glomeruli and further fixed with 4% paraformaldehyde for 1 hour at room temperature. Attached and fixed glomeruli on coverslips were then washed 3x in PBS, blocked with SEA BLOCK Blocking Buffer (PIERCE) for 40 minutes, then permeabilized with 0.5% Triton X-100 in PBS for 10 minutes. Glomeruli on coverslips were then stained using standard procedures, and imaging was performed using a Zeiss LSM 880 confocal microscope.

Confocal microscopy. Confocal imaging was performed in the Cell Biology and Imaging Core in the O'Brien Kidney Research Core, on a Zeiss LSM880 with Airyscan laser scanning microscope equipped with Plan-Apochromat 10x/0.3 NA, 20x/0.8 NA, 25x/0.8 NA and 63×/1.40 NA oil-immersion objective (ZEISS, Oberkochen, Germany). Fluorescence images were acquired using ZEN black 2.3 software with a 20x/0.8 NA or 63x/1.40 NA objective and Zeiss Immersion Oil 518F was used for the 63x/1.40 NA objective. Experiments were performed at constant room temperature. Images or regions of interest (ROIs) were further processed with ZEN 2.6 (blue edition) software.

Electron microscopy. Tissue samples were fixed with 2.5% (v/v) glutaraldehyde in 0.1M sodium cacodylate buffer (pH7.4). After three rinses with 0.1 M sodium cacodylate buffer, samples were embedded in 3% agarose and sliced into small blocks (1mm^3), rinsed with the same buffer three times and post-fixed with 1% osmium tetroxide and 0.8 % potassium ferricyanide in 0.1 M sodium cacodylate buffer for one and a half hours at room temperature. Samples were rinsed with water and then block stained with 4% uranyl acetate in 50% ethanol for two hours. They were then dehydrated with increasing concentration of ethanol, transitioned into propylene oxide, infiltrated with Embed-812 resin, and polymerized in a 60°C oven overnight. Blocks were sectioned with a diamond knife (Diatome) on a Leica Ultracut 7 ultramicrotome (Leica Microsystems) and collected onto copper grids, post stained with 2% aqueous uranyl acetate and lead citrate. Images were acquired on a JEM-1400 Plus transmission electron microscope equipped with a LaB_6 source operated at 120 kV using an AMT-BioSprint 16M CCD camera.

Bulk RNA sequencing. The total input of 100ng RNA was used for the library preparation on each sample. The library was prepared using Illumina TruSeq RNA Library Prep Kit v2 (RS-122-2001) according to Manufacturer's protocol. This protocol allows RNA input of 100ng-1000ng. Illumina UMI barcodes were used to multiplex the libraries as per the Manufacturer's instructions. The quality and quantity of each sequencing final library were

assessed using Agilent 2100 BioAnalyzer system (Agilent, CA, USA). A total of 10 nM picogreen measured library were pooled for 1.3pM loading on the sequencer. The pooled libraries were sequenced on Illumina NexSeq platform in PE75 (75 bp paired end) run with the NextSeq reagent kit v2.5 for 75 cycles. Approximately 30-40 Million sequencing reads were generated per sample for the transcriptome analysis.

Paired end demultiplexed fastq files were generated using bcl2fastq2 (Illumina, v2.17), from NextSeq550 v2.5 reagent's bcl files. Initial quality control was performed using FastQC v0.11.8 and multiqc v1.7. Fastq files were imported batch wise, trimmed for adapter sequences followed by quality trimming using CLC Genomics Workbench (CLC Bio, v23.0.3). The imported high-quality reads were mapped against gene regions and transcripts annotated by ENSEMBL v99 hg38 using the RNA-seq Analysis tool v2.7 (CLC Genomics Workbench), only matches to the reverse strand of the genes were accepted (using the strand-specific reverse option). Differential gene expression analysis between the sample groups was done using the Differential Expression for RNA-seq tool v2.8, where the normalization method was set as TMM. Differential expression between the groups was tested using a control group, outliers were downweighed, and filter on average expression for FDR correction was enabled.

Gene expression QC, quantification, and DEG analysis. Fastq reads were aligned to the mouse genome (GENCODE Version M27) followed by a multi-step quality control process, which included assessments at the read, mapping, and dataset levels according to RNA sequencing quality control methods previously outlined (63). Gene-level expression quantification utilized HTSeq, and the resulting count data were normalized using Voom. Differential gene expression analysis was performed in R using the Limma package (64). The Benjamini & Hochberg method for controlling the false discovery rate was applied as a correction factor for the adjusted p-value. Statistically significant differentially expressed genes (DEGs) were determined based on an adjusted p-value threshold of less than 0.05. All heatmaps were created using the ComplexHeatmap R package (65).

The Podocin:Nephrin ratio (PNR), a term introduced by Roger C. Wiggins, serves as a crucial marker for assessing podocyte hypertrophic stress by examining the differential mRNA expression of Podocin (NPHS2) and Nephrin (NPHS1). Under hypertrophic stress, podocytes exhibit an increase in NPHS2 and NPHS1 mRNA, with a disproportionately higher rise in NPHS2. This ratio has been shown to correlate with podocyte density, podocyte detachment, proteinuria, progressive glomerulosclerosis, and end-stage kidney disease (ESKD)(36).

Elevated PNR indicates reduced podocyte density and increased detachment, both of which contribute to proteinuria and glomerulosclerosis, ultimately progressing to ESKD. Nishizono et al. provided robust evidence supporting the association between PNR and these pathological conditions and treatment effects, underscoring its potential as a diagnostic and prognostic tool in kidney disease(66).

Integration of podocyte-specific enriched genes from NEPTUNE FSGS patients projected onto mouse models. We identified 77 patients from the NEPTUNE cohort with a diagnosis of FSGS. Molecular data in the form of microdissected bulk RNA-seq was available for analysis and was utilized for this study. An Independent Component Analysis was performed to identify clusters of co-expressed genes in an unsupervised way. ICA is a matrix decomposition method that separates multifactorial signals into additive subcomponents. Each component could be driven by latent factors such as disease, cell type, and even noise. 25 optimal modules were extracted using Python package stabilized-ica-2.0. Optimal module number was determined as described(67). We identified one module enriched for podocyte-specific genes. Because Alport nephropathy, like FSGS, is a primary podocytopathy, we utilized this module as being reflective of podocyte injury (**Supplemental Figure S8**). Furthermore, we reasoned that because injury patterns are likely to be conserved across disease types and species, identifying the presence of these genes and their differential expression across all the time points (2, 4, and 7 months) will offer a temporal perspective on how these human data enriched podocyte genes change over time. Their alteration with TUDCA therapy will provide clues to temporal changes in these genes and therapeutic potential with TUDCA or signals downstream of TUDCA.

Determining whether mouse genes associated with proteinuria are associated with Nephrotic Range Proteinuria in Humans: The above set of 253 genes associated with proteinuria in mice was then applied as a concept in Nephroseq version 4. The entry of these concept genes allows to identify the enrichment of this gene set in other glomerular disease and other CKD datasets. Specifically, we determined whether this set of mouse genes when applied to their human orthologs are enriched in cohorts with nephrotic range proteinuria. For the purpose of this analysis, we used FSGS patients from the recent paper by Mariani et al to determine whether this set of genes was significantly enriched in nephrotic range versus non-nephrotic range proteinuria(43).

Author contributions

JY and ZL conducted experiments, JY, ZL, OA, and IM acquired data, JY, ZL, MA, CAA, OA, IM, SE, MK, JMH, VN, ASN, ANC, and RTM analyzed data, LAB and PAJ provided critical methods and reagents, ASN, ANC and RTM wrote the manuscript, all authors contributed to editing the manuscript.

Acknowledgments

The work published in this manuscript were supported by the National Institutes of Health grant numbers DK083592 (to LAB PAJ, and RTM), the Charles and Jane Pak Center for Mineral Metabolism and Clinical Research (RTM, ANC), and the NEPTUNE consortium (JN, MK, SE, MA). **ASN:** ASN acknowledges support of Intramural grants from the University of Michigan O'Brien Kidney Translational Core Center P30 DK081943, 76Taubman Institute and an extramural grant from the National Institute of Health K23 DK 125529.

The Nephrotic Syndrome Study Network (NEPTUNE) is part of the Rare Diseases Clinical Research Network (RDCRN), which is funded by the National Institutes of Health (NIH) and led by the National Center for Advancing Translational Sciences (NCATS) through its Division of Rare Diseases Research Innovation (DRDRI). NEPTUNE is funded under grant number U54DK083912 as a collaboration between NCATS and the National Institute of Diabetes and Digestive and Kidney Diseases (NIDDK). Additional funding and/or programmatic support is provided by the University of Michigan, NephCure Kidney International, Alport Syndrome Foundation, and the Halpin Foundation. RDCRN consortia are supported by the RDCRN Data Management and Coordinating Center (DMCC), funded by NCATS and the National Institute of Neurological Disorders and Stroke (NINDS) under U2CTR002818.

References

1. Sharif B, and Barua M. Advances in molecular diagnosis and therapeutics in nephrotic syndrome and focal and segmental glomerulosclerosis. *Curr Opin Nephrol Hypertens.* 2018;27(3):194-200.

2. Papazachariou L, Demosthenous P, Pieri M, Papagregoriou G, Stavrou C, Zavros M, et al. Frequency of COL4A3/COL4A4 mutations amongst families segregating glomerular microscopic hematuria and evidence for activation of the unfolded protein response. Focal and segmental glomerulosclerosis is a frequent development during aging. *PLoS ONE.* 2014;9(12):e115015.

3. Groopman EE, Marasa M, Cameron-Christie S, Petrovski S, Aggarwal VS, Milo-Rasouly H, et al. Diagnostic Utility of Exome Sequencing for Kidney Disease. *N Engl J Med.* 2019;380(2):142-51.

4. Deltas C, Savva I, Voskarides K, Papazachariou L, and Pierides A. Carriers of Autosomal Recessive Alport Syndrome with Thin Basement Membrane Nephropathy Presenting as Focal Segmental Glomerulosclerosis in Later Life. *Nephron.* 2015;130(4):271-80.

5. Greka A, and Mundel P. Cell Biology and pathology of podocytes. *AnnRevPhysiol.* 2012;74:299-323.

6. Hu M, Azeloglu EU, Ron A, Tran-Ba KH, Calizo RC, Tavassoly I, et al. A biomimetic gelatin-based platform elicits a pro-differentiation effect on podocytes through mechanotransduction. *Sci Rep.* 2017;7:43934.

7. Rogg M, Maier JI, Van Wymersch C, Helmstädter M, Sammarco A, Lindenmeyer M, et al. α-Parvin Defines a Specific Integrin Adhesome to Maintain the Glomerular Filtration Barrier. *J Am Soc Nephrol.* 2022.

8. Maier JI, Rogg M, Helmstädter M, Sammarco A, Schilling O, Sabass B, et al. EPB41L5 controls podocyte extracellular matrix assembly by adhesome-dependent force transmission. *Cell Rep.* 2021;34(12):108883.

9. Schell C, and Huber TB. The Evolving Complexity of the Podocyte Cytoskeleton. *J Am Soc Nephrol.* 2017;28(11):3166-74.

10. Embry AE, Liu Z, Henderson JM, Byfield FJ, Liu L, Yoon J, et al. Similar Biophysical Abnormalities in Glomeruli and Podocytes from Two Distinct Models. *J Am Soc Nephrol.* 2018;29(5):1501-12.

11. Embry AE, Mohammadi H, Niu X, Liu L, Moe B, Miller-Little WA, et al. Biochemical and Cellular Determinants of Renal Glomerular Elasticity. *PLoS One.* 2016;11(12):e0167924.

12. Rinschen MM, Grahammer F, Hoppe AK, Kohli P, Hagman H, Kretz O, et al. YAP-mediated mechanotransduction determines the podocyte's response to damage. *Sci Signaling.* 2017;10:eaaf8165.

13. Ferrell N, Sandoval RM, Bian A, Campos-Bilderback SB, Molitoris BA, and Fissell WH. Shear stress is normalized in glomerular capillaries following ⅚ nephrectomy. *Am J Physiol Renal Physiol.* 2015;308(6):F588-93.

14. Wyss HM, Henderson JM, Byfield FJ, Bruggeman LA, Ding Y, Huang C, et al. Biophysical properties of normal and diseased renal glomeruli. *AmJPhysiol(Cell).* 2011;300:C397-C405.

15. Azeloglu EU, Hardy SV, Eungdamrong NJ, Chen Y, Jayaraman G, Chuang PY, et al. Interconnected network motifs control podocyte morphology and kidney function. *Sci Signal.* 2014;7(311):ra12.

16. Calizo RC, Bhattacharya S, van Hasselt JGC, Wei C, Wong JS, Wiener RJ, et al. Disruption of podocyte cytoskeletal biomechanics by dasatinib leads to nephrotoxicity. *Nat Commun.* 2019;10(1):2061.

17. Gyarmati G, Shroff UN, Izuhara A, Hou X, Da Sacco S, Sedrakyan S, et al. Intravital imaging reveals glomerular capillary distension and endothelial and immune cell activation early in Alport syndrome. *JCI Insight.* 2022;7(1).

18. Ding F, Wickman L, Wang SQ, Zhang Y, Wang F, Afshinnia F, et al. Accelerated podocyte detachment and progressive podocyte loss from glomeruli with age in Alport Syndrome. *Kidney Int.* 2017;92(6):1515-25.

19. Wickman L, Hodgin JB, Wang SQ, Afshinnia F, Kershaw D, and Wiggins RC. Podocyte Depletion in Thin GBM and Alport Syndrome. *PLoS One.* 2016;11(5):e0155255.

20. Kriz W, Hähnel B, Hosser H, Rösener S, and Waldherr R. Structural analysis of how podocytes detach from the glomerular basement membrane under hypertrophic stress. *Front Endocrinol (Lausanne).* 2014;5:207.

21. Cosgrove D, Kalluri R, Miner JH, Segal Y, and Borza DB. Chosing a mouse model to study the molecular pathobiology of Alport glomerulonephritis. *Kidney International.* 2007;71:615-8.

22. Andrews KL, Mudd JL, Li C, and Miner JH. Quantitative trait loci influence renal disease progression in a mouse model of Alport syndrome. *AmJPath.* 2002;160(2):721-30.

23. Miner JH, and Sanes JR. Molecular and functional defects in kidneys from mice lacking collagen ‡3(IV): implications for Alport syndrome. *JCell Biol.* 1996;135(5):1403-13.

24. Schell C, Rogg M, Suhm M, Helmstädter M, Sellung D, Yasuda-Yamahara M, et al. The FERM protein EPB41L5 regulates actomyosin contractility and focal adhesion formation to maintain the kidney filtration barrier. *Proc Natl Acad Sci U S A.* 2017;114(23):E4621-e30.

25. Pieri M, Stefanou C, Zavarinos A, Erguler K, Stylianou K, Lapathitis G, et al. Evidence for activation of the unfolded protein resppnse in collagen IV nephropathies. *JASN.* 2014;25:260-75.

26. Yu S, Gu X, Zheng Q, Liu Y, Suhas T, Du W, et al. Tauroursodeoxycholic acid ameliorates renal injury induced by COL4A3 mutation. *Kidney Int.* 2024;106(3):433-49.

27. Wang D, Mohammad M, Wang Y, Tan R, Murray LS, Ricardo S, et al. The Chemical Chaperone, PBA, Reduces ER Stress and Autophagy and Increases Collagen IV α5 Expression in Cultured Fibroblasts From Men With X-Linked Alport Syndrome and Missense Mutations. *Kidney Int Rep.* 2017;2(4):739-48.

28. Kusaczuk M. Tauroursodeoxycholate-Bile Acid with Chaperoning Activity: Molecular and Cellular Effects and Therapeutic Perspectives. *Cells.* 2019;8(12).

29. Rani S, Sreenivasaiah PK, Kim JO, Lee MY, Kang WS, Kim YS, et al. Tauroursodeoxycholic acid (TUDCA) attenuates pressure overload-induced cardiac remodeling by reducing endoplasmic reticulum stress. *PLoS One.* 2017;12(4):e0176071.

30. Panda DK, Bai X, Zhang Y, Stylianesis NA, Koromilas AE, Lipman ML, et al. SCF-SKP2 E3 ubiquitin ligase links mTORC1/ER stress/ISR with YAP activation in murine renal cystogenesis. *J Clin Invest.* 2022;132(24).

31. Uppala JK, Gani AR, and Ramaiah KVA. Chemical chaperone, TUDCA unlike PBA, mitigates protein aggregation efficiently and resists ER and non-ER stress induced HepG2 cell death. *Sci Rep.* 2017;7(1):3831.

32. Wyss HM, Henderson JM, Byfield FJ, Bruggeman LA, Ding Y, Huang C, et al. Biophysical properties of normal and diseased renal glomeruli. *Am J Physiol Cell Physiol.* 2011;300(3):C397-405.

33. Levental I, Levental KR, Klein EA, Assoian R, Miller RT, Wells RG, et al. A simple indentation device for measuring micrometer-scale tissue stiffness. *Journal of Physics: Condensed Matter.* 2010;22:191420.

34. Ge X, Zhang T, Yu X, Muwonge AN, Anandakrishnan N, Wong NJ, et al. LIM-Nebulette Reinforces Podocyte Structural Integrity by Linking Actin and Vimentin Filaments. *J Am Soc Nephrol.* 2020.

35. Liu Z, Yoon J, Wichaidit C, Jaykumar AB, Dbouk HA, Embry AE, et al. Control of Podocyte and Glomerular Capillary Wall Structure and Elasticity by WNK1 Kinase. *Front Cell Dev Biol.* 2020;8:618898.

36. Fukuda A, Wickman LT, Venkatareddy MP, Wang SQ, Chowdhury MA, Wiggins JE, et al. Urine podocin:nephrin mRNA ratio (PNR) as a podocyte stress biomarker. *Nephrol Dial Transplant.* 2012;27(11):4079-87.

37. Abrahamson DR, Hudson BG, Stroganova L, Borza DB, and St John PL. Cellular origins of type IV collagen networks in developing glomeruli. *J Am Soc Nephrol.* 2009;20(7):1471-9.

38. Pieri M, Stefanou C, Zavarinos A, Erguler K, Stylianou K, Lapathitis G, et al. Evidence for activation of the unfolded protein response in collagen IV nephropathies. *JASN.* 2014;25:260-75.

39. Wiseman RL, Mesgarzadeh JS, and Hendershot LM. Reshaping endoplasmic reticulum quality control through the unfolded protein response. *Mol Cell.* 2022;82(8):1477-91.

40. Marutani T, Yamamoto A, Nagai N, Kubota H, and Nagata K. Accumulation of type IV collagen in dilated ER leads to apoptosis in Hsp47-knockout mouse embryos via induction of CHOP. *J Cell Sci.* 2004;117(Pt 24):5913-22.

41. Lo AC, Callaerts-Vegh Z, Nunes AF, Rodrigues CMP, and D'Hooge R. Tauroursodeoxycholic acid (TUDCA) supplementation prevents cognitive impairment and amyloid deposition in APP/PS1 mice. *Neurobiology of Disease.* 2013;50:21-9.

42. Jarad G, Knutsen RH, Mecham RP, and Miner JH. Albumin contributes to kidney disease progression in Alport syndrome. *Am J Physiol Renal Physiol.* 2016;311(1):F120-30.

43. Mariani LH, Eddy S, AlAkwaa FM, McCown PJ, Harder JL, Nair V, et al. Precision nephrology identified tumor necrosis factor activation variability in minimal change disease and focal segmental glomerulosclerosis. *Kidney Int.* 2023;103(3):565-79.

44. Venkatareddy M, Wang S, Yang Y, Patel S, Wickman L, Nishizono R, et al. Estimating podocyte number and density using a single histologic section. *J Am Soc Nephrol.* 2014;25(5):1118-29.

45. Naik AS, Le D, Aqeel J, Wang SQ, Chowdhury M, Walters LM, et al. Podocyte stress and detachment measured in urine are related to mean arterial pressure in healthy humans. *Kidney Int.* 2020;98(3):699-707.

46. Cervenka L, Mitchell KD, and Navar LG. Renal function in mice: effects of volume expansion and angiotensin II. *J Am Soc Nephrol.* 1999;10(12):2631-6.

47. Rubel D, Boulanger J, Craciun F, Xu EY, Zhang Y, Phillips L, et al. Anti-microRNA-21 Therapy on Top of ACE Inhibition Delays Renal Failure in Alport Syndrome Mouse Models. *Cells.* 2022;11(4).

48. Cortes P, Zhao X, Riser BL, and Narins RG. Regulation of glomerular volume in normal and partially nephrectomized rats. *AmJPhysiol(Renal Physiol).* 1996;270:F356-F70.

49. Wiggins JE, Goyal M, Sanden SK, Wharram BL, Shedden KA, Misek DE, et al. Podocyte hypertrophy, "adaptation," and "decompensation" associated with glomerular enlargement and glomerulosclerosis in the aging rat: prevention by calorie restriction. *J Am Soc Nephrol.* 2005;16(10):2953-66.

50. Naik AS, Wang SQ, Chowdhury M, Aqeel J, O'Connor CL, Wiggins JE, et al. Critical timing of ACEi initiation prevents compensatory glomerular hypertrophy in the remaining single kidney. *Sci Rep.* 2021;11(1):19605.

51. Kashtan CE, and Gross O. Clinical practice recommendations for the diagnosis and management of Alport syndrome in children, adolescents, and young adults-an update for 2020. *Pediatr Nephrol.* 2021;36(3):711-9.

52. Desjardins M, and Bendayan M. Ontogenesis of glomerular basement membrane: structural and functional properties. *J Cell Biol.* 1991;113(3):689-700.

53. Rheault MN, Kren SM, Thielen BK, Mesa HA, Crosson JT, Thomas W, et al. Mouse model of X-linked Alport syndrome. *JASN.* 2004;15:1466-74.

54. Gale DP, Gross O, Wang F, Esteban de la Rosa RJ, Hall M, Sayer JA, et al. A Randomized Controlled Clinical Trial Testing Effects of Lademirsen on Kidney Function Decline in Adults with Alport Syndrome. *Clin J Am Soc Nephrol.* 2024.

55. Widjaja AA, Shekeran SG, Adami E, Ting JGW, Tan J, Viswanathan S, et al. A Neutralizing IL-11 Antibody Improves Renal Function and Increases Lifespan in a Mouse Model of Alport Syndrome. *J Am Soc Nephrol.* 2022.

56. Keestra-Gounder AM, Byndloss MX, Seyffert N, Young BM, Chávez-Arroyo A, Tsai AY, et al. NOD1 and NOD2 signalling links ER stress with inflammation. *Nature.* 2016;532(7599):394-7.

57. Wang W, Zhao J, Gui W, Sun D, Dai H, Xiao L, et al. Tauroursodeoxycholic acid inhibits intestinal inflammation and barrier disruption in mice with non-alcoholic fatty liver disease. *Br J Pharmacol.* 2018;175(3):469-84.

58. Kim S, Ramalho TR, and Haynes CM. Regulation of proteostasis and innate immunity via mitochondria-nuclear communication. *J Cell Biol.* 2024;223(3).

59. Yerlikaya A. Heme-regulated inhibitor: an overlooked eIF2α kinase in cancer investigations. *Med Oncol.* 2022;39(5):73.

60. Schlondorff D. Preparation and study of isolated glomeruli. *Methods in Enzymology.* 1990;191:130-40.

61. Naldini L, Blömer U, Gallay P, Ory D, Mulligan R, Gage FH, et al. In vivo gene delivery and stable transduction of nondividing cells by a lentiviral vector. *Science.* 1996;272(5259):263-7.

62. Shankland SJ, Pippin JW, Reiser J, and Mundel P. Podocytes in culture: past, present, and future. *Kidney Int.* 2007;72(1):26-36.

63. Hong C, Eichinger F, Atta MG, Estrella MM, Fine DM, Ross MJ, et al. Viral associations with kidney disease diagnosis and altered kidney metatranscriptome by kidney function. *Kidney Int.* 2023;103(1):218-22.

64. Ritchie ME, Phipson B, Wu D, Hu Y, Law CW, Shi W, et al. limma powers differential expression analyses for RNA-sequencing and microarray studies. *Nucleic Acids Res.* 2015;43(7):e47.

65. Gu Z. Complex heatmap visualization. *iMeta.* 2022;1(3):e43.

66. Nishizono R, Kikuchi M, Wang SQ, Chowdhury M, Nair V, Hartman J, et al. FSGS as an Adaptive Response to Growth-Induced Podocyte Stress. *J Am Soc Nephrol.* 2017;28(10):2931-45.

67. Kairov U, Cantini L, Greco A, Molkenov A, Czerwinska U, Barillot E, et al. Determining the optimal number of independent components for reproducible transcriptomic data analysis. *BMC Genomics.* 2017;18(1):712.

Figures

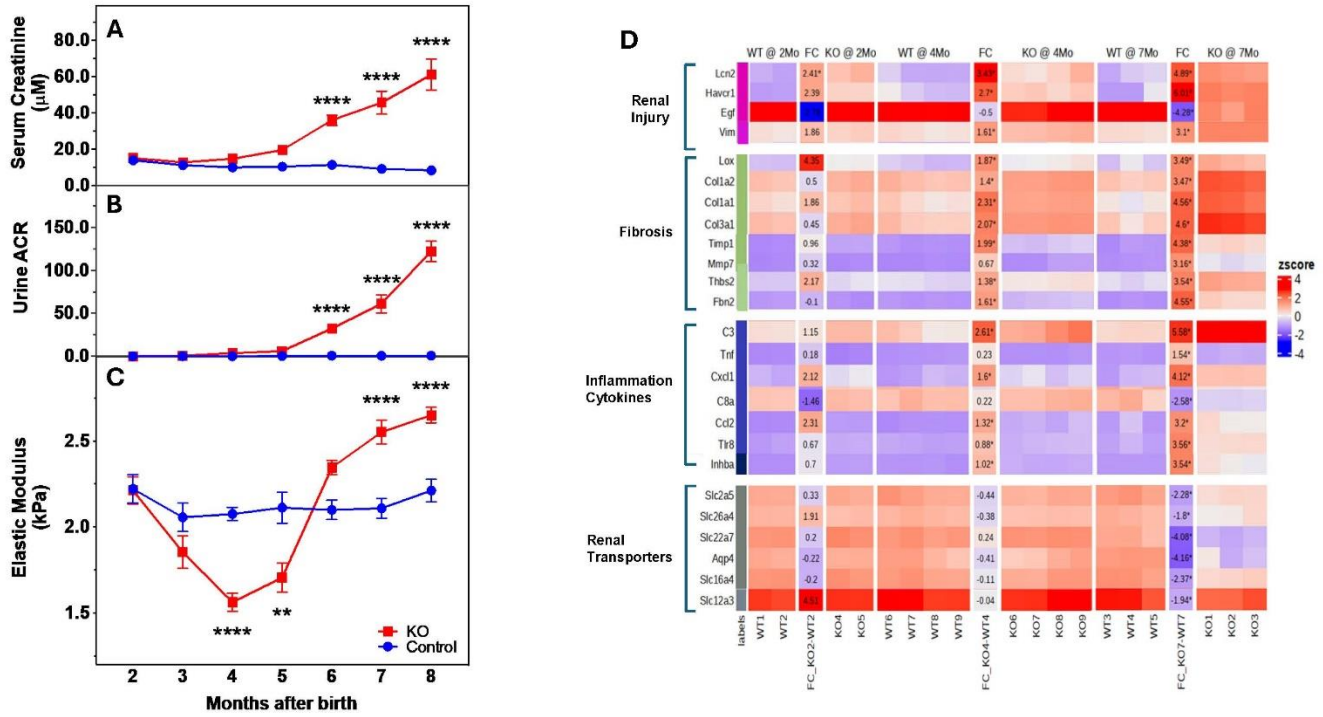

Figure 1. Measurement of serum creatinine (**A**), urine ACR (**B**), and glomerular elastic modulus (E, Young's modulus) (**C**) in *Col4α3*$^{-/-}$ (KO, red) mice over the course of renal disease compared to wildtype or heterozygote controls (Control, blue). Beginning two months after birth, serum creatinine (µM) and urine ACR (mg/g) were measured monthly through eight months. Glomerular E (kPa) was measured in mice sacrificed at indicated time point using microindentation of isolated glomeruli. Each point in graphs shows average E values from 4 - 12 different mice with 6 – 10 glomeruli measured in each mouse. Significance was determined by 2-way ANOVA using Graphpad; **P<0.01, ****P<0.0001. **(D)** Differentially expressed genes in KO kidneys at 2, 4, and 7 months compared to age-matched WT. N=2 per group at 2 months, 4 per group at 4 months, and 3 per group at 7 months.

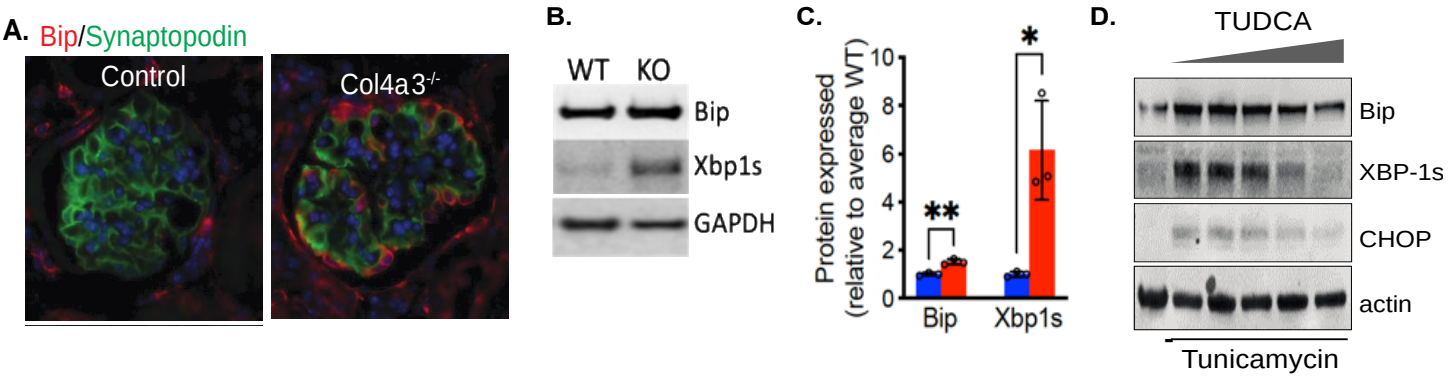

Figure 2. Evidence of UPR activation in glomeruli and podocytes from *Col4α3*$^{-/-}$ mice. A) Immunofluorescence images of Bip and Synaptopodin staining in 4-month T and *Col4α3*$^{-/-}$ mouse glomeruli, **B)** Blots of UPR markers in podocyte cell lines under basal conditions derived from WT and *Col4α3*$^{-/-}$ (KO) mice. The cells were maintained under standard conditions, harvested in RIPA buffer at 7% confluence, and the crude extract was immunoblotted with antibodies against Bip, Xbp1s, and GAPDH. The conditionally immortalized WT and *Col4α3*$^{-/-}$ cells were developed from primary cultures of 3-month WT and Col4α3$^{-/-}$ glomeruli. **C)** Comparison of Bip and Xbp1s protein expression from B (N=3, normalized to WT). **D)** Efficacy of TUDCA for blocking tunicamycin-induced of UPR marker expression in WT podocytes. Podocytes were treated with tunicamycin 1 μg/ml and then increasing concentrations of TUDCA from 1 - 4 mM for four hours.

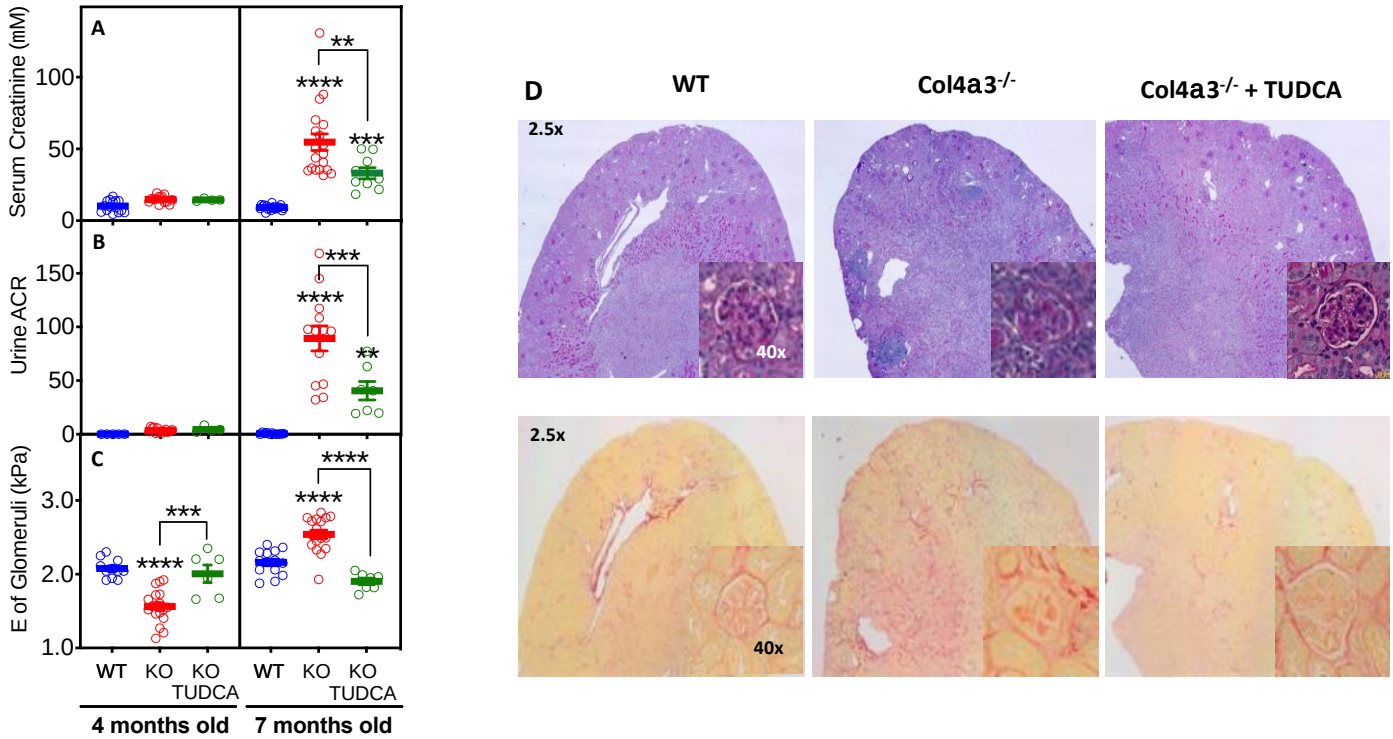

Figure 3. TUDCA treatment slows progression of renal disease and moderates the changes in E in Col4α3$^{-/-}$ mice. Col4α3$^{-/-}$ (KO) mice were treated from weaning (approximately 4 weeks), with 0.8% TUDCA mouse chow (KO TUDCA) until sacrifice. At 4 and 7 months of age, serum creatinine (μM) (**2A**), urine ACR (**2B**), and glomerular elastic modulus (E, kPa) (**2C**) was measured in WT (Blue), KO (Red) and TUDCA treated KO animals (Green). In A and B, each circle represents measurement from one mouse, and in C, each circle represents E measured from an average of 6-10 individual glomeruli from a single mouse. Significance was determined by ANOVA and multiple comparisons test using GraphPad; **P<0.01, ***P<0.001, ****P<0.0001. **2D.** Comparison of kidney cortex from WT, *Col4α3$^{-/-}$* (KO), and TUDCA treated *Col4α3$^{-/-}$* (KO) animals. Top row, sections from 7-month mice are stained with PAS and bottom row sections from 7-month mice are stained with picrosirius red. Insets in each panel show representative glomeruli from each condition.

Fibrosis	WT (N)	KO (N)	KO-TUDCA (N)
Col1α1	1 (4)	55.5 ± 13 (3)	26.2± 6.2 (4)
Col1α2	1 (4)	29.6 ± 7.3 (5)	13.9 ± 3.2 (4)
Col3α1	1 (4)	74.1 ± 31.9 (5)	31.9 ± 2.4 (4)
Lox	1 (4)	29.7 ± 7.4 (3)	13..3 ± 7.6 (4)
Loxl2	1 (4)	21.5 ± 7.1 (3)	6.7 ± 3.1 (4)
Cytokines			
TGF-β1	1 (4)	4.8 ± 0.8 (4)	3.0 ± 0.7 (4)
TNF-α	1 (4)	30.3 ± 7.9 (3)	14.3 ± 3.0 (4)
IGF-1	1 (4)	9.81 ± 2.23 (4)	5.93 ± 1.72 (4)
Chemokines/Receptors			
Cxcl1	1 (4)	45.0 ± 11.4 (4)	20.9 ± 2.11 (3)
Ccl2	1 (4)	41.5 ± 9.3 (4)	34.6 ± 5.68 (4)
Ccr2	1 (4)	15.0 ± 3.45 (5)	4.04 ± 1.57 (3)
Injury Markers			
EGF	1 (4)	0.20 ± 0.1 (5)	0.7 ± 0.2 (4)
Ccn1 (Cyr61)	1 (4)	4.46 ± 0.6 (3)	2.0 ± 1.0 (4)

Table 1. Summary of qRT-PCR of selected fibrosis, cytokine, chemokine, or injury-related genes in 7-month *Col4α3*$^{-/-}$ mice without (KO) and with (KO-TUDCA) TUDCA treatment, compared to age-matched WT littermates. All values in KO and KO-TUDCA groups represent fold change from WT ± SD, and were significantly different from Control, as determined by ANOVA. The number of samples in each group is shown in parentheses after the values (N).

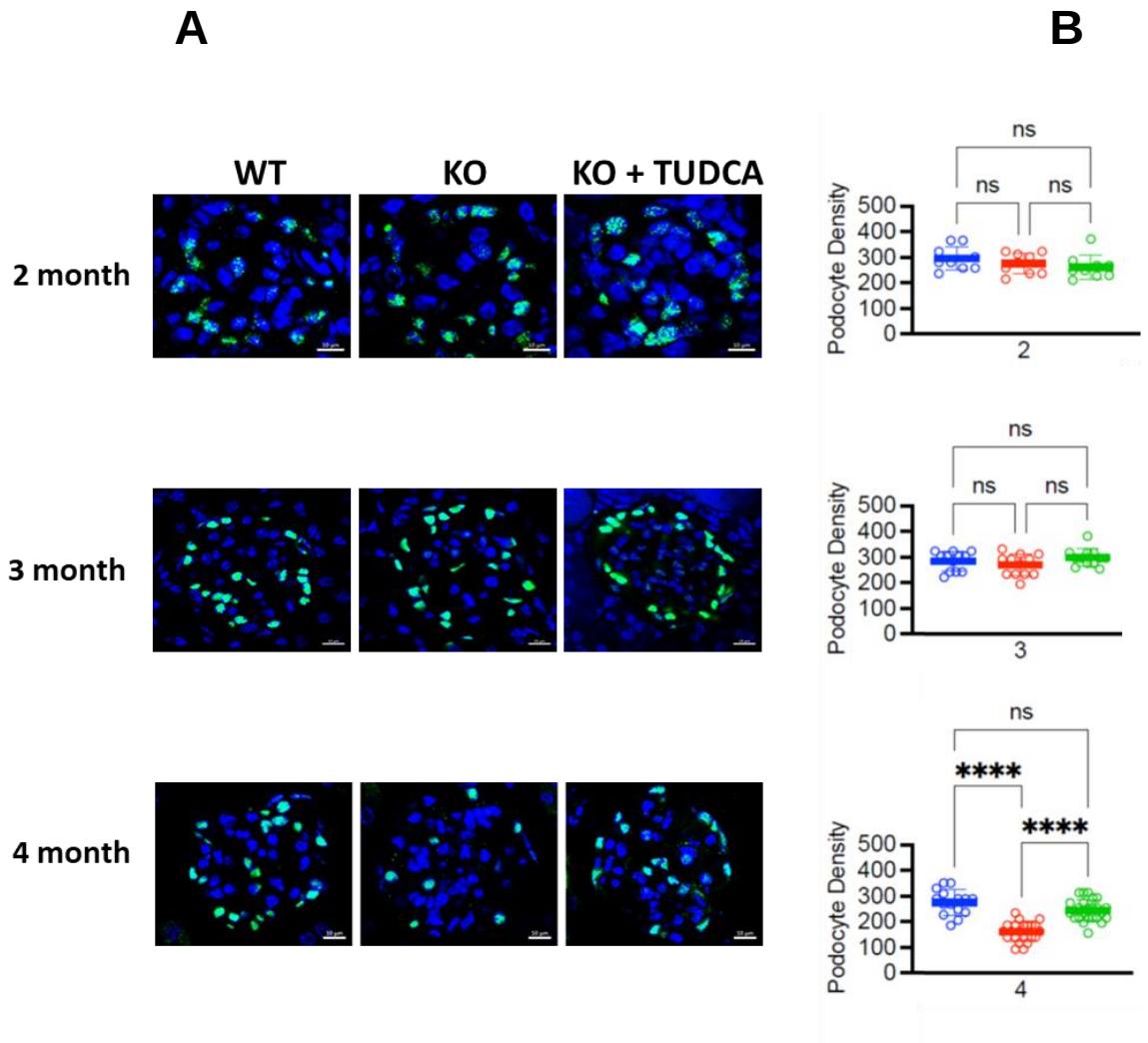

Figure 4. TUDCA reduces podocyte loss from *Col4α3*$^{-/-}$ mouse glomeruli. A) Representative glomeruli in kidney sections from WT, *Col4α3*$^{-/-}$ (KO), and TUDCA-treated *Col4α3*$^{-/-}$ (KO+TUDCA) mice from 2, 3, and 4-month-old mice were stained for WT-1 and DAPI. Scale bar: 10 µm. **B)** Summary of podocyte density analysis. WT – Blue, *Col4α3*$^{-/-}$ - Red, and *Col4α3*$^{-/-}$ - T Green. The number of WT-1 and DAPI-positive nuclei in 20 glomeruli from 3 mice were counted and used for podocyte density calculations. Each dot represents the number of WT-1 positive nuclei in a single glomerulus. Data are shown as mean ± SEM and significance was determined by ordinary one-way ANOVA, followed by Dunnett's multiple comparisons test; ****P<0.0001. At 2 months - Podocytes/10^6 µm^3 ± SD, WT 296±44, *Col4α3*$^{-/-}$ 276±39, and *Col4α3*$^{-/-}$+T 262±45). At 3 months - Podocytes/10^6 µm^3 ± SD, WT 285±35, *Col4α3*$^{-/-}$ 270±40, and *Col4α3*$^{-/-}$+T 299±32). At 4 months, Podocytes/10^6 µm^3 ± SD, WT 276±48, *Col4α3*$^{-/-}$ 162±37, and *Col4α3*$^{-/-}$+T 246±40).

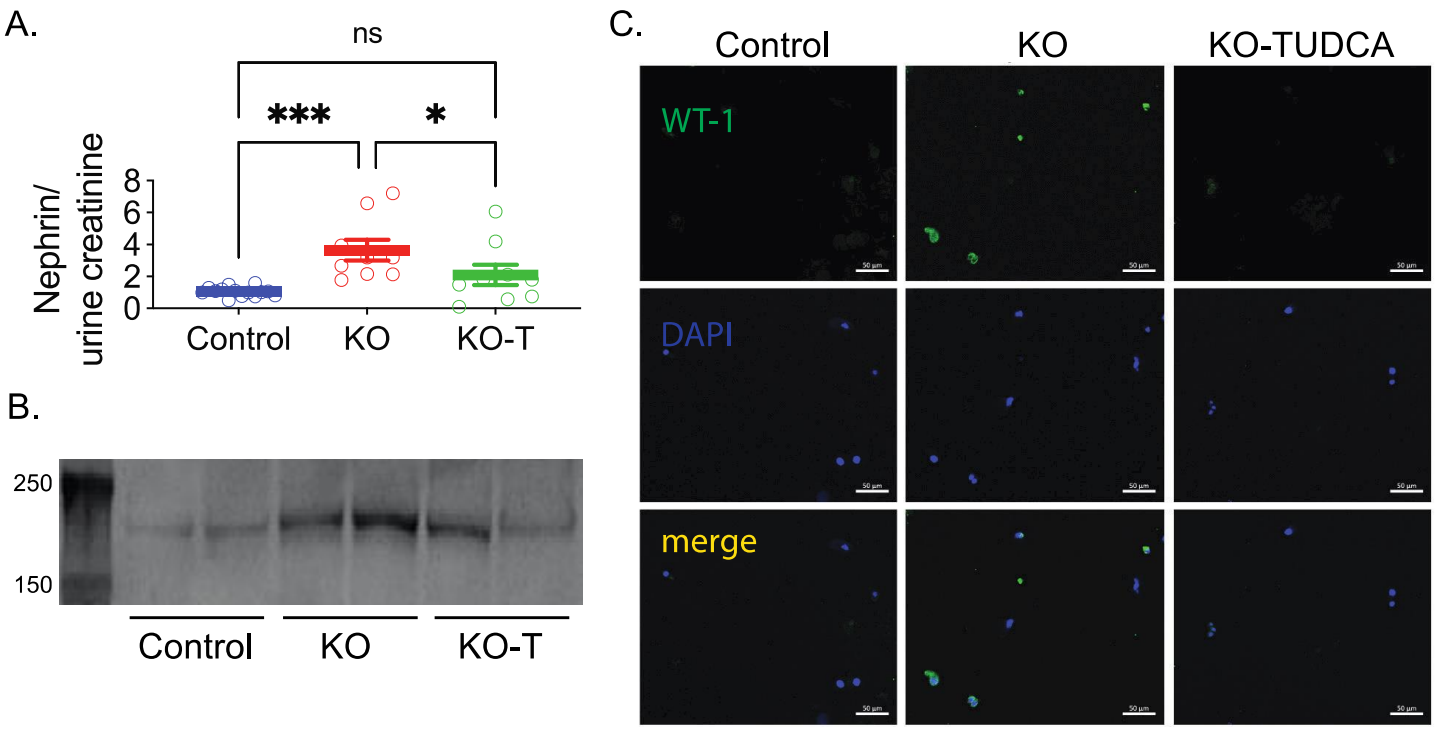

Figure 5. Glomerular capillary deformability and podocytes adhesion. WT (Control), *Col4α3*$^{-/-}$ (KO), and *Col4α3*$^{-/-}$ -T (KO-TUDCA) mice were injected (IP) with approximately 1 ml of saline, and urine was collected over the subsequent two hours. The urine samples were normalized for creatinine, immunoblotted for nephrin, and quantitated with densitometry. The urine pellet was stained for WT-1 and DAPI. **A**) shows aggregate data for all sample groups expressed as nephrin/creatinine (arbitrary densitometry units for nephrin) for each sample group. WT – Blue, *Col4α3*$^{-/-}$ - Red, and *Col4α3*$^{-/-}$ - T Green. Each point represents a sample from a single mouse, bar indicates mean ± SEM. Significance was determined by ordinary one-way ANOVA, followed by Tukey's multiple comparisons test; *P<0.05, ***P<0.001. **B**) Representative urine nephrin immunoblot with duplicate samples, loading normalized with creatinine. **C**) representative urine sediment samples stained for WT-1 and DAPI.

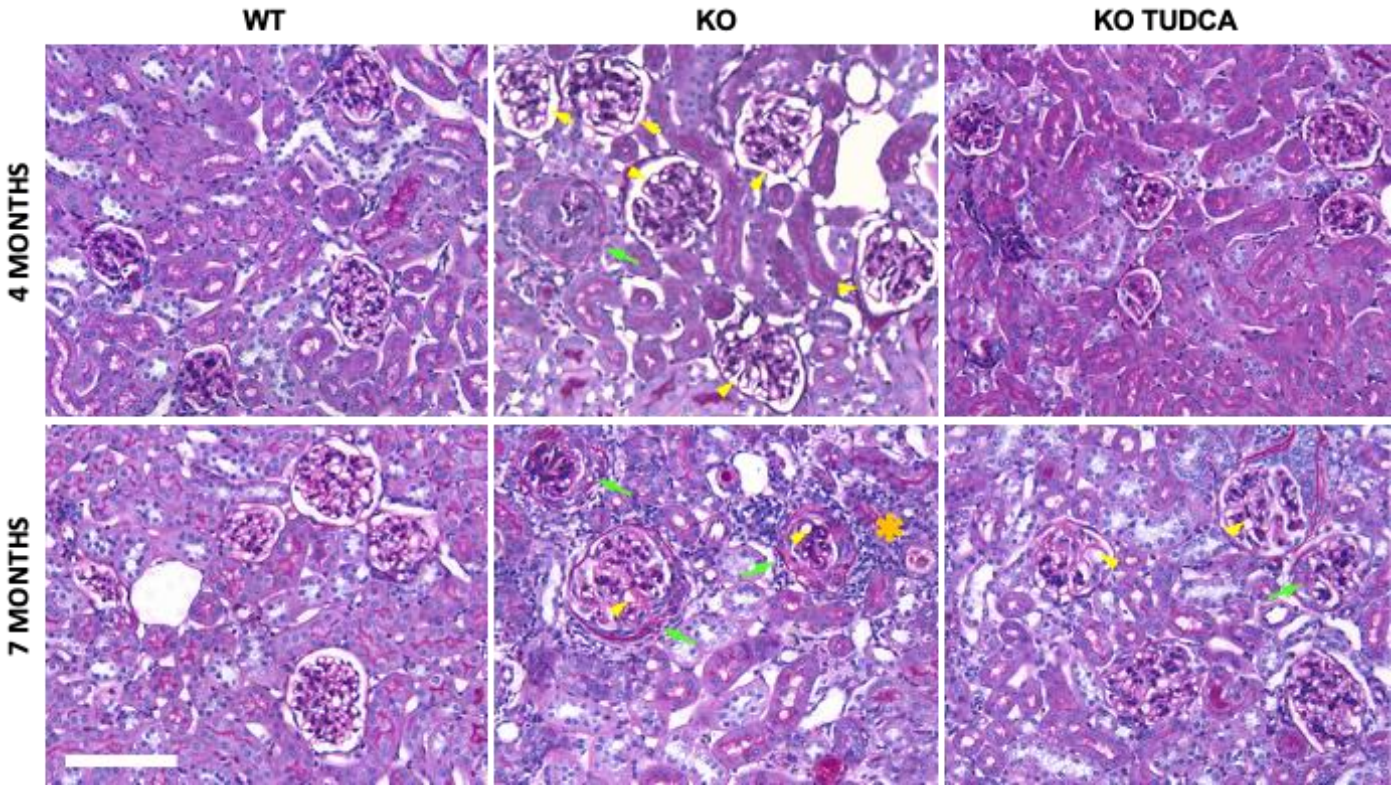

Figure 6. Brightfield photomicrographs of PAS-stained kidney sections from 4 month-old (top row) and 7-month-old (bottom row) WT, *Col4α3*$^{-/-}$ (KO), and TUDCA-treated *Col4α3*$^{-/-}$ (KO TUDCA) mice. The 4-month KO image shows glomerular enlargement and focal proliferative glomerular lesions (green arrow), and dilation of glomerular capillary lumens (yellow arrowheads) that are not observed in Control (top left) or the TUDCA treated KO mice (top right). The 7-month KO mice (bottom center) show more extensive glomerular proliferative lesion development (green arrows), with proliferation composed predominantly of epithelial cells filling Bowman's space, along with patchy areas of tubular atrophy and interstitial fibrosis and chronic inflammation (orange asterisk). The section from the 7-month TUDCA-treated mice show evidence of less severe glomerular injury. Scale bar = 200 µm for all images.

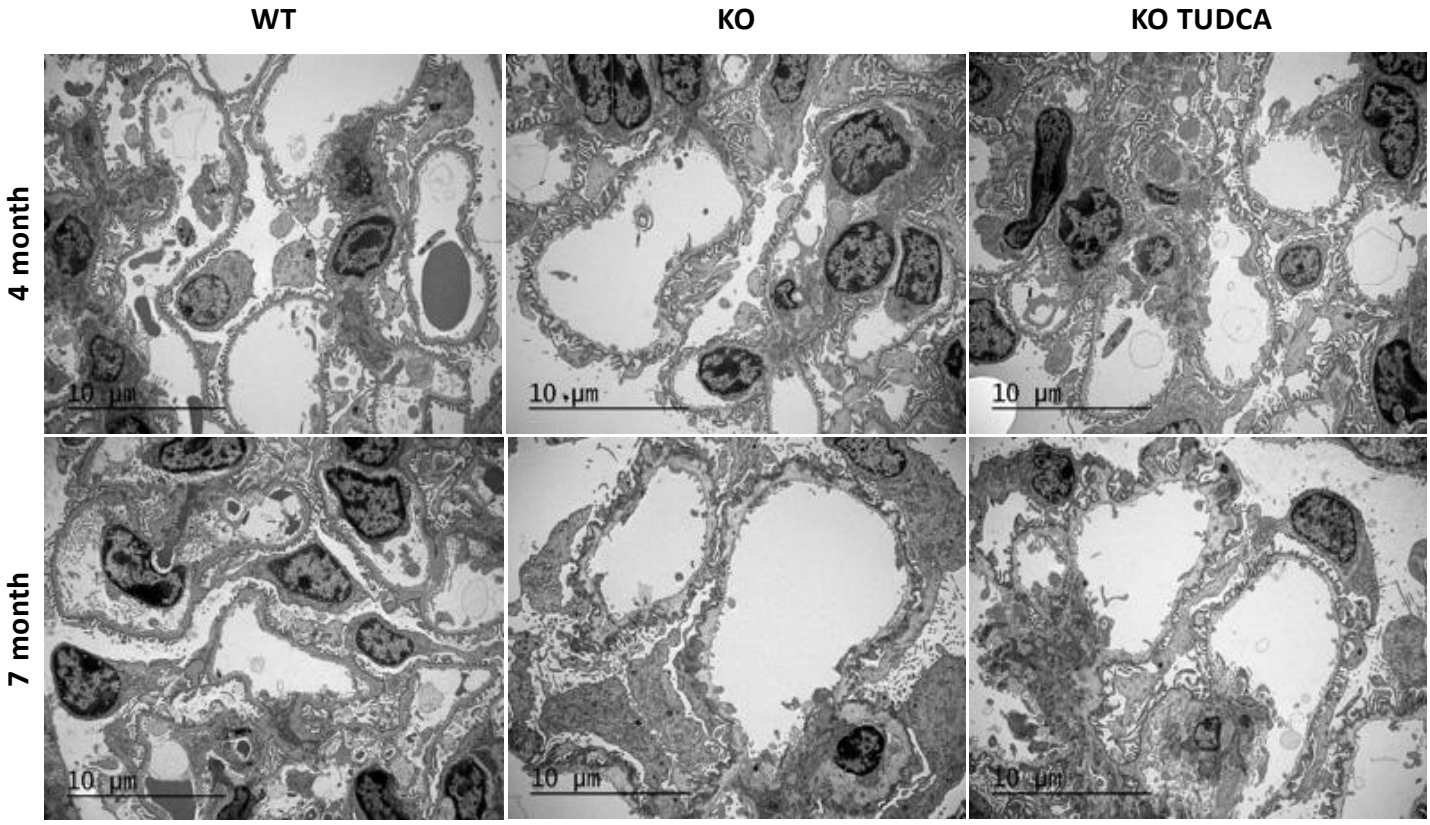

Figure 7. Transmission Electron micrographs of mouse kidneys, showing glomerular changes at 4 (top row) and 7 (bottom row) months in WT, *Col4α3*$^{-/-}$ (KO), and TUDCA-treated *Col4α3*$^{-/-}$ (KO TUDCA) mice. At 4 months, glomeruli of KO mice (top center) and KO TUDCA mice (top right) reveal features of segmental podocyte injury, including mild segmental podocyte foot process effacement, more extensive but segmental foot process irregularity, and mild microvillous change. These podocyte changes are concurrent with segmentally prominent "knob-like" subepithelial basement redundancy, characteristic of the *Col4α3*$^{-/-}$ mouse model. WT mice (top left) show none of these changes. At 7 months (bottom row), KO mice (bottom center) reveal more severe and widespread podocyte injury, demonstrated by extensive podocyte foot process effacement and irregularity, cellular hypertrophy, and microvillous change. There are also comparable glomerular basement membrane changes including extensive subepithelial basement redundancy and segmental "basket weave", and segmental glomerular capillary loop dilation. In contrast, 7 month KO TUDCA mice (bottom right) show podocyte and glomerular basement membrane changes that are similar in nature to those of the KO mice but are less extensive and more segmental. None of these changes are seen in Control mice (bottom left). All images are the same magnification – scale bar = 10 µm.

A.

Gene	2 Mo	4 Mo	7 Mo
TNF	ND	ND	2.9
IfnG	ND	ND	ND
TGFB1	NS	ND	3.46
IL6	1.14	1.77	2.26
IL1B	NS	ND	4.86
Stat3	1.4	1.6	2.54
SmarcA4	NS	1.17	1.51
Kras	NS	ND	1.7
IL4	ND	ND	ND
Osm	NS	ND	1.42
Nfkb	ND	1.56	3.55
Stat1	NS	ND	1.57
Erbb2	NS	ND	ND
Tp53	ND	ND	ND

B.

Gene	2 Mo	4 Mo	7 Mo
CCL2	NS	2.5	9.2
CCL4	ND	ND	ND
CCL5	NS	ND	2.81
CCL11	2.6	ND	ND
CCL22	NS	ND	4.03
CXCL1	3.34	3.03	17.4
CXCL10	ND	ND	1.57
IL1RN	NS	ND	6.73
IL7	NS	ND	1.77
MMP2	1.62	2.64	13.4
MMP9	NS	ND	2.07
TIMP1	2.13	3.97	20.8
TIMP2	NS	1.77	4.2

Table 2. Upstream activators (A) and downstream TNF pathway markers (B) from the NEPTUNE dataset characterizing FSGS and MCD outcome. In A, the upstream activators were identified in the poor prognosis cluster representing disease progression, and the genes in B represent down-stream targets of TNF were identified in the same NEPTUNE population in renal parenchyma and urine proteins(43). The values represent DEGs from the *Col4α3*$^{-/-}$ mice at 2, 4, or 7 months and are expressed as fold-increase over respective age-matched WT and are FCLog 10. All values are significant ($p<0.05$) or shown as NS - not significant, or ND - Not Differentially Expressed.